

Apparent horizon formation in the head-on collision of gyratons

Hirotaka Yoshino, Andrei Zelnikov, and Valeri P. Frolov

Department of Physics, University of Alberta, Edmonton, Alberta, Canada T6G 2G7

(Received 26 March 2007; published 5 June 2007)

The gyron model describes a gravitational field of an object moving with the velocity of light which has finite energy and spin distributed during some finite time interval L . A gyron may be considered as a classical toy model for a quantum wave packet of high-energy particles with spin. In this paper we study a head-on collision of two gyratons and black hole formation in this process. The goal of this study is to understand the role of the gravitational spin-spin interaction in the process of mini-black-hole formation in particle collisions. To simplify the problem, we consider several gyron models with special profiles of the energy and spin density distribution. For these models we study the apparent horizon (AH) formation on the future edge of a spacetime region before interaction. We demonstrate that the AH forms only if the energy duration and the spin are smaller than some critical values, while the length of the spin distribution should be at least of the order of the system gravitational radius. We also study gravitational spin-spin interaction in the head-on collision of two gyratons under the assumption that the values of gyron spins are small. We demonstrate that the metric in the interaction region for such gyratons depends on the relative helicities of incoming gyratons, and the collision of gyratons with oppositely directed spins allows the AH formation in a larger parameter region than in the collision of the gyratons with the same direction of spins. Some applications of the obtained results to the mini-black-hole production at the Large Hadron Collider in TeV gravity scenarios are briefly discussed.

DOI: [10.1103/PhysRevD.75.124005](https://doi.org/10.1103/PhysRevD.75.124005)

PACS numbers: 04.70.Bw, 04.25.Nx, 04.30.Nk, 04.50.+h

I. INTRODUCTION

The black hole formation in high-energy particle collisions is an important issue especially in the context of TeV gravity scenarios [1–3]. In the theory with large extra dimensions, the Planck energy could be of the order of TeV, and collisions of particles with the center-of-mass energy greater than the Planckian one will occur in future accelerators such as the Large Hadron Collider (LHC) at CERN [4]. A detailed study of mini-black-hole production, especially at the threshold of this effect, would require the complete theory of quantum gravity. However, if the mass of a created black hole is much larger than the Planck mass, one can use a semiclassical approximation to describe such processes. In this approximation, the black hole formation in particle collision and its subsequent decay in the process of the Hawking evaporation are studied in the framework of the (semi)classical general relativity. The apparent horizon (AH) is a useful tool for estimation of the black hole production rate in this approximation, because the existence of an AH is a sufficient condition for the black hole formation.

The first work along this line was done by Eardley and Giddings [5] in the four-dimensional case. Since the high-energy particles are relativistic, they used the Aichelburg-Sexl (AS) metric [6] to describe the gravitational field of such particles before their collision. The AS metric can be obtained by boosting a Schwarzschild black hole to the speed of light and keeping the energy p of the boosted black hole fixed. The gravitational field of the AS particle is a shock and it is localized on the null plane ($u = 0$ for one of the particles and $v = 0$ for the other one). One of the null generators on each of the null planes represents a

particle trajectory, while its gravitational field is distributed in the transverse plane orthogonal to the direction of motion. Two AS particles do not interact before the collision and the metric outside of the interacting region is known explicitly. Eardley and Giddings analytically studied the AH on some slice ($u = 0 \geq v$ and $v = 0 \geq u$) and derived the maximal impact parameter b_{\max} for the AH formation. The quantity $\sigma_{\text{AH}} = \pi b_{\max}^2$ gives the lower bound on the cross section of the black hole production.

The results of [5] were generalized by one of us and Nambu [7] for the mini-black-hole formation in the higher-dimensional spacetimes. In this work the numerical calculations were used. Later, one of us and Rychkov [8] improved these results by studying the AH on the futuremost slice that can be adopted without the knowledge of the interacting region (i.e., $u = 0 \leq v$ and $v = 0 \leq u$). Using this approach the stronger lower bound $\sigma_{\text{AH}}/\pi[r_h(2p)]^2 \approx 2\text{--}3$ on the cross section of the black hole production in the collision of AS particles was obtained for spacetime dimensionality $D = 5\text{--}11$.

Certainly the model of colliding AS particles is oversimplified. The AS particles are assumed to be neutral and spinless. In reality, all the known elementary particles have spin and most of them have either electric or color charge as well.

Charged particles have additional charge-charge interaction besides the gravitational interaction. Moreover, their gravitational interaction can also be modified. The latter effect was discussed to some extent by one of us and Mann [9]. In that paper a boosted Reissner-Nordström metric was used as the model of an ultrarelativistic charged particle and the head-on collision in a spacetime with an arbitrary

number of dimensions was studied. The results obtained in that paper indicate that the charge makes the AH formation more difficult. It was also argued that the effects of the quantum electrodynamics could change the results. The results of [9] were later used by Gingrich [10] who reconsidered the black hole production rate at the LHC.

In the quantum mechanical description, the colliding particles are characterized by wave packets which have a finite duration in time [11]. To take into account this effect as well as to include spin-spin interaction, in this paper we study head-on collisions of two gyratons.

The gyraton model was proposed in [12]. The motivation of this paper was to find the gravitational field generated by a beam pulse of spinning radiation with a finite time duration, which is propagating at the speed of light. In the gyraton model, the metric outside of the source satisfies the vacuum Einstein equations and the gravitational field is distributed in the plane transverse to the direction of motion. Unlike an AS particle, the gravitational field of a gyraton is not a shock wave but has the finite duration in time. A gyraton may have spin which manifests itself in the dragging-into-rotation effect. The AS particle metrics can be obtained from the gyraton solutions if the duration is taken infinitely small and the spin vanishes. General properties of gyraton metrics were studied in detail in [13]. Electrically charged gyratons and gyratons in the supergravity were discussed in [14,15], respectively. Gyration solutions can also be generalized to the case when the spacetime is asymptotically anti-de Sitter [16,17].

Colliding gyratons which we consider in this paper differ from the AS particles both by the presence of spin and the finite duration in time. Let us discuss briefly what kind of new features one can expect. The first natural question is: Can one include spin effects in the interaction between highly nonrelativistic particles by boosting the Kerr metric? Such boosted Kerr black hole solutions were considered, e.g. in [18–20], in the four-dimensional spacetime and in [21] in higher dimensions. The main problem in this approach is the following. In order to have a well-defined limit for the boosted metric, one needs to keep the energy p of the system fixed, so that the mass of the black hole $M = \gamma^{-1}p$ must vanish when the γ -factor infinitely grows. If one assumes that the spin s remains finite in this limit, the rotation parameter $a = s/M$ infinitely grows, so that the metric describes a naked singularity. The radius of the ring singularity is of the order of a and also infinitely grows. The latter problem can be avoided by assuming that the rotation parameter a remains finite in the infinite boost limit, as it was done in the above references. Although finite results different from the AS particle can be obtained by this procedure, fixing a means that the spin $s = aM$ of the boosted object vanishes. Furthermore, in this limit we have an object of typical size a , which does not satisfy the requirement that we would like to have a pointlike object. Thus a boosted

Kerr black hole does not provide one with a suitable model for an ultrarelativistic particle with spin, e.g. for a photon. In the gyraton model the spin is easily included.

There is another aspect of the high-energy particle collision which the gyraton model may help to understand better. Recently, the validity of an AS particle as the model of a high-energy elementary particle was questioned in [22]. In this model the curvature invariants at the moment of the collision of the two planes, representing the colliding particles, are infinite, so that formally higher-curvature quantum corrections may be important. This problem was discussed in [11]. It was argued that the quantum effects, such as the finite size and finite duration in time of the incoming wave packets, can help to solve this problem. The quantum-to-classical transition in the description of the mini-black-hole formation in the particle collision is an interesting open question. We do not address it in our paper, but instead we use the gyraton model in order to discuss how the finiteness of the duration in time of the colliding objects modifies the results of the AS approximation. In such an approach, the gyratons might be considered as an effective model for the quantum wave packets.

With these motivations we study the AH formation in the head-on collision of gyratons. For simplicity we consider the four-dimensional case. The paper is organized as follows. In the next section, we introduce several gyration models: a gyraton without spin, its AS limit, and spinning gyratons. As for spinning gyratons, we consider two types depending on relative locations of the energy and spin profiles. Then we set up five cases of head-on collisions of gyratons. In Sec. III, we derive an AH equation on the future edge of the spacetime region before interaction, $u = 0 \leq v$ and $v = 0 \leq u$. We present the numerical results of this study in Sec. IV. The conditions on the spin and on the energy and spin durations for the AH formation are obtained for each of the collision cases. Then in Sec. V we focus our attention on the study of the spin-spin interaction. In general, this is a complicated problem, since it requires the knowledge of the metric in the region of interaction. To obtain it, one needs to solve nonlinear Einstein equations. We simplify the problem by assuming that the spins of the interacting objects are small and solve the equations by using a method of perturbation. Then we study again the AH formation on the new slice that is the future edge of the solved region. In the adopted approximation we obtain spin-spin interaction corrections to the mini-black-hole production. Section VI contains a summary of the results and a discussion of their possible applications for the study of mini-black-hole production at the LHC.

II. SYSTEM SETUP

In this section, we set up the problem of the head-on collisions of two gyratons. We first review the gyration

model in a four-dimensional spacetime in Sec. II A. The gyraton has the total energy p and the spin J which are distributed in time. Their time profiles are characterized by two functions. We introduce four kinds of gyratons by specifying these two functions. Next in Sec. II B, we introduce a system of null geodesic coordinates, which is necessary for specifying the slice to study the AH existence. It is also useful for clarifying the gravitational field of gyratons. In Sec. II C, we set up five cases of head-on collisions of two gyratons, using the introduced four gyratons.

A. The gyraton model

The gyraton model was proposed in [12]. In that paper, the gravitational field generated by a beam pulse of spinning radiation was first studied in the weak field approximation and then the exact solutions of the Einstein equations were obtained, which reduce to the approximate solution at a far distance from the source. These solutions were obtained in any number of spacetime dimensions. In particular, a four-dimensional gyraton has the metric

$$ds^2 = -d\bar{u}d\bar{v} + d\bar{r}^2 + \bar{r}^2 d\bar{\phi}^2 - 4G(2p \log \bar{r} \chi_p(\bar{u}) d\bar{u} - J \chi_j(\bar{u}) d\bar{\phi}) d\bar{u}. \quad (1)$$

This metric represents a spacetime in which a segment-shaped source located at $\bar{r} = 0$ with the total energy p and the spin J is propagating at the speed of light along $\bar{u} = \text{const}$. The existence of the term $d\bar{\phi}d\bar{u}$ in Eq. (1) indicates the presence of a dragging-into-rotation effect generated by the spin source. The functions $\chi_p(\bar{u})$ and $\chi_j(\bar{u})$ are arbitrary functions satisfying the normalization conditions

$$\int \chi_p(\bar{u}) d\bar{u} = \int \chi_j(\bar{u}) d\bar{u} = 1. \quad (2)$$

They represent the energy and spin density profiles, respectively.

Introducing the new coordinates $\bar{x} := (\bar{r} \cos \bar{\phi}, \bar{r} \sin \bar{\phi})$, nonzero components of the energy-momentum tensor of the gyraton are calculated as

$$T_{\bar{u}\bar{u}} = p \chi_p(\bar{u}) \delta(\bar{x}) + \pi G J^2 \chi_j^2(\bar{u}) \delta^2(\bar{x}), \quad (3)$$

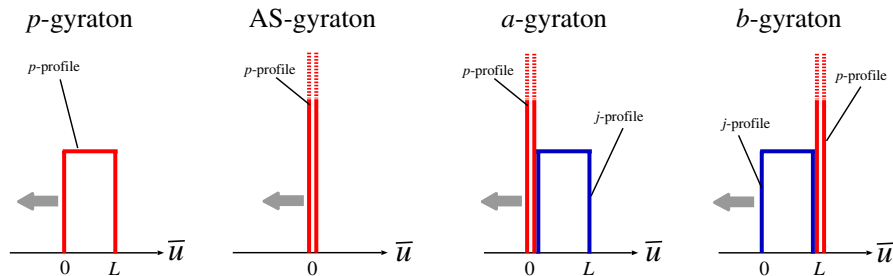


FIG. 1 (color online). The energy and spin density profiles, $\chi_p(\bar{u})$ and $\chi_j(\bar{u})$, for the p -, AS-, a -, and b -gyratons, respectively. The grey arrows show the directions of propagation.

$$T_{\bar{u}a} = \frac{J}{4} \chi_j(\bar{u}) \epsilon_{ab} \partial_b \delta(\bar{x}). \quad (4)$$

These formulas show that the source has an infinitely narrow shape. For a realistic beam pulse, the source should have a finite radius $\bar{r} = \bar{r}_s$ and the metric will take a different form from Eq. (1) for $\bar{r} < \bar{r}_s$. Therefore Eq. (1) is considered to be the metric outside of the source $\bar{r} \geq \bar{r}_s$. In this paper, we do not take account of this finiteness (in space) of the beam pulse for simplicity and adopt Eq. (1) for arbitrary values of \bar{r} (i.e., $\bar{r}_s = 0$).

Hereafter we adopt the gravitational radius of $2p$, i.e. $r_h(2p) = 4Gp$, as the unit of the length. In this length unit, the gyraton metric is represented as

$$ds^2 = -d\bar{u}d\bar{v} + d\bar{r}^2 + \bar{r}^2 d\bar{\phi}^2 - 2 \log \bar{r} \chi_p(\bar{u}) d\bar{u}^2 + 2j \chi_j(\bar{u}) d\bar{\phi} d\bar{u}. \quad (5)$$

Here, j is a dimensionless quantity defined by $j := J/2pr_h(2p)$ and we use j as a parameter to specify the spin of the gyraton.

The gyraton model is specified by determining the functions $\chi_p(\bar{u})$ and $\chi_j(\bar{u})$. The interaction between two gyratons with arbitrary profiles $\chi_p(\bar{u})$ and $\chi_j(\bar{u})$ is a quite complicated problem which, in the general case, requires numerical calculations. Hence, it is natural to consider first the simplest profiles for which the null geodesic coordinates can be studied analytically. For this reason, in this paper we consider four types of gyratons whose energy and spin profiles are as shown in Fig. 1. We will explain them one by one in the following. For convenience, we introduce the following function:

$$\vartheta(\bar{u}, L) = \frac{1}{L} (\theta(\bar{u}) - \theta(\bar{u} - L)), \quad (6)$$

where $\theta(\bar{u})$ is the Heaviside step function. Its integral over \bar{u} is 1, and in the limit $L \rightarrow 0$ it gives a δ -function.

1. p -gyraton

The first one is a gyraton without spin with energy duration L . For this model, we adopt

$$\begin{cases} \chi_p(\bar{u}) = \vartheta(\bar{u}, L), \\ \chi_j(\bar{u}) = 0. \end{cases} \quad (7)$$

This model is useful for studying the effect of the energy duration on the AH formation. We simply call it a “spinless gyraton” or a “ p -gyrator” because it has only one parameter, energy p .

2. AS-gyrator

The second one is an Aichelburg-Sexl (AS) particle [6] with

$$\begin{cases} \chi_p(\bar{u}) = \delta(\bar{u}), \\ \chi_j(\bar{u}) = 0. \end{cases} \quad (8)$$

This is the limit $L \rightarrow 0$ of the p -gyrator. Hereafter we call it an “AS-gyrator” for short.

3. a -gyrator and b -gyrator

The remaining two gyrators, which are referred to as an “ a -gyrator” and a “ b -gyrator,” have nonzero spin. We adopt the following functions of $\chi_p(\bar{u})$ and $\chi_j(\bar{u})$ for a - and b -gyratons:

$$a\text{-gyrator: } \begin{cases} \chi_p(\bar{u}) = \delta(\bar{u}), \\ \chi_j(\bar{u}) = \vartheta(\bar{u}, L); \end{cases} \quad (9)$$

$$b\text{-gyrator: } \begin{cases} \chi_p(\bar{u}) = \delta(\bar{u} - L), \\ \chi_j(\bar{u}) = \vartheta(\bar{u}, L), \end{cases} \quad (10)$$

In these two models, L represents the spin duration and the energy has zero duration. We call them an a -gyrator and a b -gyrator, respectively, because for the a -gyrator, the spin source comes *after* the energy source, while for the b -gyrator, the spin source comes *before* the energy source. These two models are useful for studying the effect of the spin and its density duration on the AH formation. By comparing the results of a - and b -gyratons, we can understand to what extent the obtained results depend on relative positions of the energy and spin density profiles. Each of the gyrators is reduced to an AS-gyrator if we take $j = 0$.

Readers might wonder why we do not adopt $\chi_p(\bar{u}) = \chi_j(\bar{u}) = \vartheta(\bar{u}, L)$ for spinning gyrators. This is because of a technical problem. In the next subsection, we derive a coordinate system based on the null geodesic congruences. This coordinate system can be analytically derived for a - and b -gyratons, but not for $\chi_p(\bar{u}) = \chi_j(\bar{u}) = \vartheta(\bar{u}, L)$.

B. Null geodesic coordinates

In this subsection, we introduce null geodesic coordinates, which are very useful for specifying the slice on which we study the AH. We introduce new coordinates (u, v, r, ϕ) by

$$\begin{aligned} \bar{u} = u, \quad \bar{v} = v + F(u, r), \quad \bar{r} = G(u, r), \\ \bar{\phi} = \phi + H(u, r). \end{aligned} \quad (11)$$

We assume that the two coordinate systems coincide for $\bar{u} = u \leq 0$ and hence $F = H = 0$ and $G = r$ for $u \leq 0$. For $u \geq 0$, we require a line $v, r, \phi = \text{const}$ to be a null geodesic and the coordinate u to be its affine parameter. This requirement is realized if and only if the following relations are satisfied:

$$H_{,u} = -\frac{j\chi_j(u)}{G^2}, \quad (12)$$

$$F_{,u} = G_{,u}^2 - 2\chi_p(u)\log G - \frac{j^2\chi_j^2(u)}{G^2}, \quad (13)$$

$$F_{,r} = 2G_{,u}G_{,r}. \quad (14)$$

These relations determine F , G , and H . In terms of these functions, the metric takes the form

$$ds^2 = -dudv + G_{,r}^2 dr^2 + G^2(d\phi + H_{,r}dr)^2. \quad (15)$$

Eliminating F from Eqs. (13) and (14), we find

$$G_{,uu} = -\frac{\chi_p(u)}{G} + \frac{j^2\chi_j^2(u)}{G^2}. \quad (16)$$

Once this equation is solved, one can find H by solving Eq. (12) and determine all the coefficients in the metric (15).

1. p -gyrator and AS-gyrator

For a spinless gyrator, using Eq. (7), we find

$$G(u, r) = \begin{cases} \tilde{G}(u, r), & (0 \leq u \leq L), \\ \tilde{G}_{,u}(L, r)(u - L) + \tilde{G}(L, r), & (L \leq u), \end{cases} \quad (17)$$

where

$$\tilde{G}(u, r) := r \exp(-[\text{erf}^{-1}(y)]^2), \quad (18)$$

$$y := \sqrt{\frac{2}{\pi L}} \frac{u}{r}. \quad (19)$$

Here, the function $\text{erf}^{-1}(y)$ denotes the inverse function of the error function: $x = \text{erf}^{-1}(y)$ is equivalent to

$$y = \text{erf}(x) := \int_0^x \frac{2}{\sqrt{\pi}} \exp(-t^2) dt. \quad (20)$$

In the limit $L \rightarrow 0$, the function G reduces to

$$G(u, r) = r - u/r, \quad (0 \leq u), \quad (21)$$

and the metric (15) coincides with the AS-gyrator in the null geodesic coordinates [8,22].

We should point out that there is a coordinate singularity at

$$u = \begin{cases} \sqrt{\pi L/2}r, & (0 \leq u \leq L), \\ L - \tilde{G}(L, r)/\tilde{G}_{,u}(L, r), & (L \leq u), \end{cases} \quad (22)$$

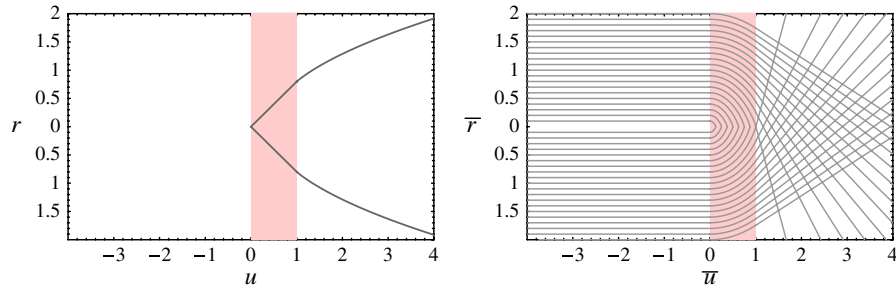


FIG. 2 (color online). The left plot shows the coordinate singularity in the (u, r) coordinates where $G = 0$ for a p -gyrator with $L = 1$. The lines $r = \text{const}$ are null geodesics and they hit the coordinate singularity. The right plot shows the light rays in the (\bar{u}, \bar{r}) coordinates. The light rays with an identical r value bend due to an attractive force and focus to one point on a symmetry axis, which corresponds to $G = 0$.

where $G = 0$. The shape of the singularity is shown by a solid line at the left plot of Fig. 2. In order to understand the meaning of this singularity, it is useful to consider null geodesics $v, r, \phi = \text{const}$. These null geodesics plunge into the coordinate singularity. Let us go back to the original $(\bar{u}, \bar{v}, \bar{r}, \bar{\phi})$ coordinates. The trajectories of the light rays in the coordinates (\bar{u}, \bar{r}) are shown in the right plot of Fig. 2. Because of the gravitational effect of the gyrator energy, the proper circumference of a congruence of light rays with an identical r value becomes small as \bar{v} is increased and eventually becomes zero. This is where the congruence hits the coordinate singularity in the (u, v, r, ϕ) coordinates. Thus, the coordinate singularity corresponds to the symmetry axis and therefore we call it the *focusing singularity*.

2. a-gyrator

Now we turn to the spinning a -gyrator. Using Eq. (9), Eqs. (12) and (16) are solved as

$$G(u, r) = \begin{cases} \tilde{G}(u, r) & (0 \leq u \leq L), \\ \tilde{G}_{,u}(L, r)(u - L) + \tilde{G}(L, r), & (L \leq u); \end{cases} \quad (23)$$

$$H(u, r) = \begin{cases} \tilde{H}(u, r), & (0 \leq u \leq L), \\ \tilde{H}(L, r), & (L \leq u), \end{cases} \quad (24)$$

where

$$\tilde{G}(u, r) := r \sqrt{\frac{j^2/L^2 + [(1 + j^2/L^2)(u/r^2) - 1]^2}{1 + j^2/L^2}}; \quad (25)$$

$$\tilde{H}(u, r) := \arctan \frac{j/L}{1 - r^2/u}. \quad (26)$$

In this case, there are two coordinate singularities. One is the singularity at

$$u = \frac{r^2(1 - r^2/L)}{1 + j^2/L^2 - r^2/L}, \quad (L \leq u), \quad (27)$$

where $G = 0$, and the other is at

$$u = \begin{cases} (1 + j^2/L^2)^{-1/2} r^2, & (0 \leq u \leq L), \\ L - \tilde{G}_{,r}(L, r)/\tilde{G}_{,ur}(L, r), & (L \leq u), \end{cases} \quad (28)$$

where $G_{,r} = 0$. The two coordinate singularities are shown in the left plot of Fig. 3. A light ray $v, r, \phi = \text{const}$ plunges into one of the two singularities. The propagation of light rays in the (\bar{u}, \bar{r}) coordinates is shown in the right plot of Fig. 3. Because there is the energy distribution at $\bar{u} = 0$,

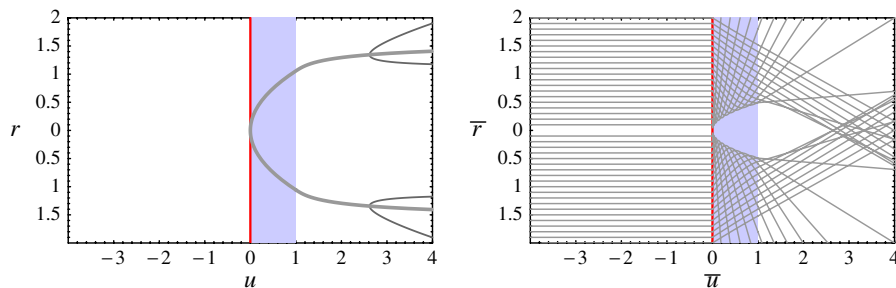
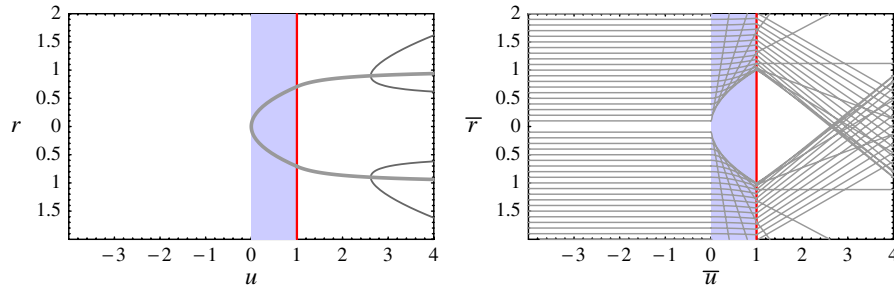


FIG. 3 (color online). The left plot shows the coordinate singularities in the (u, r) coordinates where $G = 0$ (dark gray lines) and $G_{,r} = 0$ (light gray line) for an a -gyrator with $L = 1$. The lines $r = \text{const}$ are null geodesics and they hit one of the two coordinate singularities. The right plot shows the propagation of light rays in the (\bar{u}, \bar{r}) coordinates. Light rays with a large r value focus to one point, which corresponds to $G = 0$. On the other hand, light rays with a small r value bend outward due to a repulsive force around the center. Then two neighboring light rays cross each other, which corresponds to $G_{,r} = 0$.

FIG. 4 (color online). The same as Fig. 3 but for a b -gyration.

the light rays bend quickly there. Then the light rays with a sufficiently large r value focus to one point and this is the focusing singularity $G = 0$. On the other hand, around the center, the gravitational field generated by the spin source is repulsive and the light rays of a small r value bend outward. Because of this effect, the neighboring light rays cross with each other and this is where the congruence hits the coordinate singularity $G_{,r} = 0$. Therefore we call it the *crossing singularity*.

3. b -gyration

Finally, we obtain the formulas for G and H of a spinning b -gyration. They are found by solving Eqs. (12) and (16) using Eq. (10). The result is

$$G(u, r) = \begin{cases} \tilde{G}(u, r), & (0 \leq u \leq L), \\ \frac{(j^2 - Lr^2)(u-L)}{Lr\sqrt{r^2 + j^2}} + \tilde{G}(L, r), & (L \leq u); \end{cases} \quad (29)$$

$$H(u, r) = \begin{cases} \tilde{H}(u, r), & (0 \leq u \leq L), \\ \tilde{H}(L, r), & (L \leq u), \end{cases} \quad (30)$$

where

$$\tilde{G}(u, r) := r\sqrt{1 + \frac{j^2/L^2}{(r^2/u)^2}}, \quad (31)$$

$$\tilde{H}(u, r) := -\arctan\frac{j/L}{r^2/u}. \quad (32)$$

Similarly to the a -gyration, there are the focusing singularity at

$$u = \frac{r^2(r^2/L + 1)}{r^2/L - j^2}, \quad (L \leq u), \quad (33)$$

and the crossing singularity at

$$u = \begin{cases} (L/|j|)r^2, & (0 \leq u \leq L), \\ L - \tilde{G}_{,r}(L, r)/\tilde{G}_{,ur}(L, r), & (L \leq u). \end{cases} \quad (34)$$

The shape of the two singularities in (u, r) coordinates and the propagation of light rays in (\bar{u}, \bar{r}) coordinates are shown in Fig. 4.

C. Gyration collisions

Consider two gyrations and assume that each of them belongs to one of the four types described above. We obtain several different configurations for the collisions of these gyrations. To illustrate main features of these collisions, in this subsection we set up five cases of the head-on collision of two gyrations which are of the most interest. The incoming gyrations are referred to as gyration 1 and gyration 2. Let us divide a spacetime for the two-gyration system into four regions:

$$\begin{aligned} \text{region I: } (u \leq 0, v \leq 0), & \quad \text{region II: } (u \geq 0, v \leq 0), \\ \text{region III: } (u \leq 0, v \geq 0), & \quad \text{region IV: } (u \geq 0, v \geq 0). \end{aligned} \quad (35)$$

Because the gyrations propagate at the speed of light, they do not interact with each other before the collision. Thus we can use the metric of the gyration 1 in regions I and II and the metric of the gyration 2 in regions I and III (by changing u and v). Then, the metric of the system is given as

$$ds^2 = \begin{cases} -dudv + dr^2 + r^2d\phi^2, & (\text{region I}), \\ -dudv + G_{,r}^{(1)}(u, r)^2dr^2 + G^{(1)}(u, r)^2(d\phi + H_{,r}^{(1)}(u, r)dr)^2, & (\text{region II}), \\ -dudv + G_{,r}^{(2)}(v, r)^2dr^2 + G^{(2)}(v, r)^2(d\phi + H_{,r}^{(2)}(v, r)dr)^2, & (\text{region III}). \end{cases} \quad (36)$$

The metric of region IV is unknown, because the interaction between the two gyrations determines its structure through the Einstein equations.¹

¹In Sec. IV, we will solve the Einstein equation in a part of region IV in a specific case, when spins are small.

In the previous subsection, we introduced four gyration models, i.e., a p -gyration, an AS-gyration, an a -gyration, and a b -gyration. Using these models, we will consider five cases of collision. The first one, which we call case (0), is the collision of two identical spinless p -gyrations. For both $G^{(1)}$ and $G^{(2)}$, we use the formula of G for the

p -gyrator (17)–(19). The energy p determines the scale, so that the only essential parameter which specifies the system is the energy duration L .

In the next two cases (1a) and (1b), we consider collisions of a spinning gyrator (a - and b -gyrator, respectively) with an AS-gyrator. In both cases, we assume that incoming gyrators have the same energy, and only a gyrator 1 has the spin j . These are interpreted as collisions of a spinning particle and a particle without spin. For $G^{(1)}$ and $H^{(1)}$, we use the formulas (23)–(26) of G and H for a -gyrator in the (1a) case, and use the formulas (29)–(32) of G and H for b -gyrator in the (1b) case. For $G^{(2)}$, the formula (21) of G for AS-gyrator is used in both cases. The essential parameters which specify the system are the spin j and its duration L for a gyrator 1.

In the remaining two cases (2a) and (2b), we study collisions of two a -gyratons and two b -gyratons, respectively. These are interpreted as collisions of two spinning particles. In these cases, the incoming gyrators are assumed to have the same energy p and the same spin duration L . As for the spin values, we assume that the gyrator 1 has the spin j and the gyrator 2 has the spin σj , where $\sigma = \pm 1$. Therefore two spins have the same absolute value $|j|$ and have either the same sign or different signs. For the choice $\sigma = +1$, two spins have the same direction (i.e. helicities have opposite signs), and for the choice $\sigma = -1$ two spins have opposite directions (i.e. helicities have the same sign). For $G^{(1)}$ and $H^{(1)}$, we use the formulas (23)–(26) of G and H for a -gyrator in the (2a) case, and use the formulas (29)–(32) of G and H for b -gyrator in the (2b) case. For $G^{(2)}$ and $H^{(2)}$, we use the formulas of G and H for a - and b -gyratons with j replaced by σj in the (2a) and (2b) cases, respectively. The essential parameters which specify the system are the spin j of gyrator 1, the relative directions of two spins σ , and the spin duration L of each incoming gyrator. In the study of Secs. III and IV, the condition for AH formation in the slice $u = 0 \leq v$ and $v = 0 \leq u$ will turn out to be independent of σ , and hence the essential parameters are reduced to j and L . The sign of σ will become important in the study of the spin-spin interaction in Sec. V.

All five cases are schematically illustrated in Fig. 5.

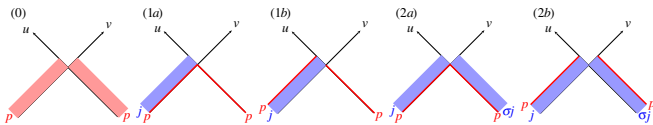


FIG. 5 (color online). The five cases of gyrator collision that we study in this paper. In case (0), two identical p -gyratons collide. In cases (1a) and (1b), a - and b -gyratons with spin j collide with an AS particle, respectively. In cases (2a) and (2b), two a - and b -gyratons with spins j and σj ($\sigma = \pm 1$) collide, respectively.

III. FINDING THE APPARENT HORIZON

The apparent horizon (AH) Σ is a compact two-dimensional spacelike surface for which the family of outgoing null rays emitted orthogonally to Σ has zero expansion. We study the AH on the slice $u \geq 0 = v$ and $v \geq 0 = u$. Figure 6 shows a schematic picture of the AH for colliding gyrators. The AH consists of two parts:

$$\begin{cases} u = h^{(1)}(r), & (u > 0 = v), \\ v = h^{(2)}(r), & (v > 0 = u). \end{cases} \quad (37)$$

These parts are connected at $u = v = 0$. Each surface has the other end at the focusing singularity. Because the focusing singularity is just one point for the same r value, the surface given by Eq. (37) is a two-dimensional closed spacelike surface.

Because the AH equations and the outer boundary conditions for $h^{(1)}$ and $h^{(2)}$ have the same form, we only consider $h(r) := h^{(1)}(r)$ and denote $G = G^{(1)}$ and $H = H^{(1)}$. The metric in the neighborhood of $v = 0 < u$ is given by

$$ds^2 = -dudv + G_{,r}^2 dr^2 + G^2(d\phi + H_{,r} dr)^2. \quad (38)$$

Let us consider a point $(u, r, \phi) = (h(R), R, \Phi)$. The local light cone with the apex at this point is

$$(u - h(R))v = G_{,r}^2(r - R)^2 + G^2[(\phi - \Phi) + H_{,r}(r - R)]^2. \quad (39)$$

We find the envelope of the local light cones by taking the derivative of Eq. (39) with respect to R and Φ . The tangent vector of the null geodesic congruence in the (u, v, r, ϕ) coordinate is

$$k^\mu = \left(\frac{h_{,r}^2}{2G_{,r}^2}, 2, \frac{h_{,r}}{G_{,r}^2}, -\frac{H_{,r}}{G_{,r}^2} h_{,r} \right). \quad (40)$$

Now we calculate the expansion. The induced metric on the $v = \text{const}$ surface is given by $d\gamma^2 = G_{,r}^2 dr^2 + G^2(d\phi + H_{,r} dr)^2$, and its determinant γ is $\sqrt{\gamma} = G_{,r} G$.

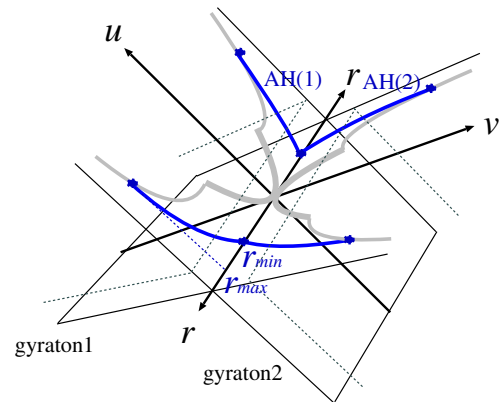


FIG. 6 (color online). The schematic picture of the AH in the slice $u \geq 0 = v$ and $v \geq 0 = u$.

Let us consider a rectangular coordinate domain with apices at the four points P_1, P_2, P_3 , and P_4 :

$$(r, \phi) = \begin{cases} P_1: (R_+, \Phi_+), \\ P_2: (R_+, \Phi_-), \\ P_3: (R_-, \Phi_+), \\ P_4: (R_-, \Phi_-). \end{cases} \quad (41)$$

Here $R_{\pm} = R \pm \Delta r/2$ and $\Phi_{\pm} = \Phi \pm \Delta \phi/2$. The proper area $\Delta A(0)$ of this domain is

$$\Delta A(0) = G_{,r} G|_{(h(R), R)} \Delta r \Delta \phi. \quad (42)$$

The null geodesics passing through the apices are

$$(r, \phi) = \begin{cases} P'_1: (R_+ + k^r(R_+)\lambda, \Phi_+ + k^\phi(R_+)\lambda), \\ P'_2: (R_+ + k^r(R_+)\lambda, \Phi_- + k^\phi(R_+)\lambda), \\ P'_3: (R_- + k^r(R_-)\lambda, \Phi_+ + k^\phi(R_-)\lambda), \\ P'_4: (R_- + k^r(R_-)\lambda, \Phi_- + k^\phi(R_-)\lambda), \end{cases} \quad (43)$$

where λ is an affine parameter. In what follows, we keep terms up to first order in λ . The coordinate shape of the domain surrounded by the four apices after evolution is a parallelogram as indicated by the vectors

$$\overrightarrow{P'_2 P'_1} = \overrightarrow{P'_4 P'_3} = (0, \Delta \phi), \quad (44)$$

$$\overrightarrow{P'_3 P'_1} = \overrightarrow{P'_4 P'_2} = ((1 + \partial_r k^r \lambda) \Delta r, \partial_r k^\phi \lambda \Delta r). \quad (45)$$

The coordinate area of the domain is $(1 + \partial_r k^r \lambda) \Delta r \Delta \phi$ and the proper area of the domain is

$$\begin{aligned} \Delta A(\lambda) &= (G_{,r} G)|_{(h(R) + k^u(R)\lambda, R + k^r(R)\lambda)} (1 + \partial_r k^r \lambda) \Delta r \Delta \phi \\ &= \Delta A(0) \left[1 + \left(\frac{G_{,ru} k^u + G_{,rr} k^r}{G_{,r}} \right. \right. \\ &\quad \left. \left. + \frac{G_{,u} k^u + G_{,r} k^r}{G} + \partial_r k^r \right) \lambda \right]. \end{aligned} \quad (46)$$

Hence, the condition $d\Delta A/d\lambda = 0$ implies

$$h_{,rr} + h_{,r} \left[-\frac{(3/2)G_{,ru} h_{,r} + G_{,rr}}{G_{,r}} + \frac{(1/2)G_{,u} h_{,r} + G_{,r}}{G} \right] = 0. \quad (47)$$

This equation determines the AH surface Σ .

Let us discuss now the boundary conditions at the outer boundary $r = r_{\max}$. By the continuity of the surface, the AH should cross the coordinate singularity at $r = r_{\max}$:

$$G(h(r_{\max}), r_{\max}) = 0. \quad (48)$$

The continuity of k^μ also must be imposed, because the surface has a delta-functional expansion if k^μ is discontinuous. Going back to the $(\bar{u}, \bar{v}, \bar{r}, \bar{\phi})$ coordinate, the continuity can be imposed as $k^{\bar{r}} = 0$ by the axisymmetry. This is equivalent to

$$h_{,r}(r_{\max}) = -2G_{,r}/G_{,u}. \quad (49)$$

The other condition for the continuity of k^μ is that $k^{\bar{\phi}}$ should take a finite value. But this is automatically satisfied since the condition $H_{,u} = 0$ at the focusing singularity implies that $k^{\bar{\phi}} = 0$.

Now we turn to the boundary conditions at the inner boundary $r = r_{\min}$. The inner boundary conditions depend on both $h^{(1)}$ and $h^{(2)}$. By continuity of the surface, both sides of the AH should cross $u = v = 0$ at $r = r_{\min}$, and thus

$$h^{(1)}(r_{\min}) = h^{(2)}(r_{\min}) = 0. \quad (50)$$

Also the null tangent vectors $k^{(1)\mu}$ and $k^{(2)\mu}$ of two surfaces should be parallel at $r = r_{\min}$ so that there is no delta-functional expansion. $k^{(1)\mu}$ and $k^{(2)\mu}$ are given by

$$k^{(1)\mu} = \left(2, \frac{h_{,r}^{(1)2}}{2}, h_{,r}^{(1)}, 0 \right), \quad k^{(2)\mu} = \left(\frac{h_{,r}^{(2)2}}{2}, 2, h_{,r}^{(2)}, 0 \right), \quad (51)$$

and $k^{(1)} \parallel k^{(2)}$ is equivalent to

$$h_{,r}^{(1)}(r_{\min}) h_{,r}^{(2)}(r_{\min}) = 4. \quad (52)$$

The numerical procedure for defining the AH is straightforward. First, we choose some value of r_{\max} and solve $h(r)$ with the outer boundary conditions (48) and (49). When $h(r)$ becomes zero at $r = r_{\min}$, we check whether the inner boundary condition (52) is satisfied. Iterating these steps for various values of r_{\max} , we determine whether the AH exists and find its location.

Note that H does not appear in the AH equation and the boundary conditions. This means that the dragging-into-rotation effect causes a change in the shear but not in the expansion. Thus on the slice we have adopted, the condition for the AH formation does not depend on the sign of j in the cases (1a) and (1b). In cases (2a) and (2b), it does not depend also on the relative directions of two spins σ . Therefore in the next section j is assumed to be positive without loss of generality and we do not specify the value of σ when the numerical results are shown.

IV. NUMERICAL RESULTS

In this section, we present the numerical results of the AH studies. The results for case (0), cases (1a) and (1b), and cases (2a) and (2b) are provided in Secs. IVA, IV B, and IV C, respectively.

A. Collision of gyratons without spin

We begin with case (0), the collision of two identical spinless p -gyratons with energy duration L . Figure 7 shows top views of the AH for $L = 0.5, 1.0$, and 1.423 . For $0 \leq L \leq 1.423$, we found only one solution, and therefore there is no inner boundary of the trapped region. For $L = 1.423$, the AH intersects the focusing singularity at $u \simeq L$ and almost touches the source of the energy which

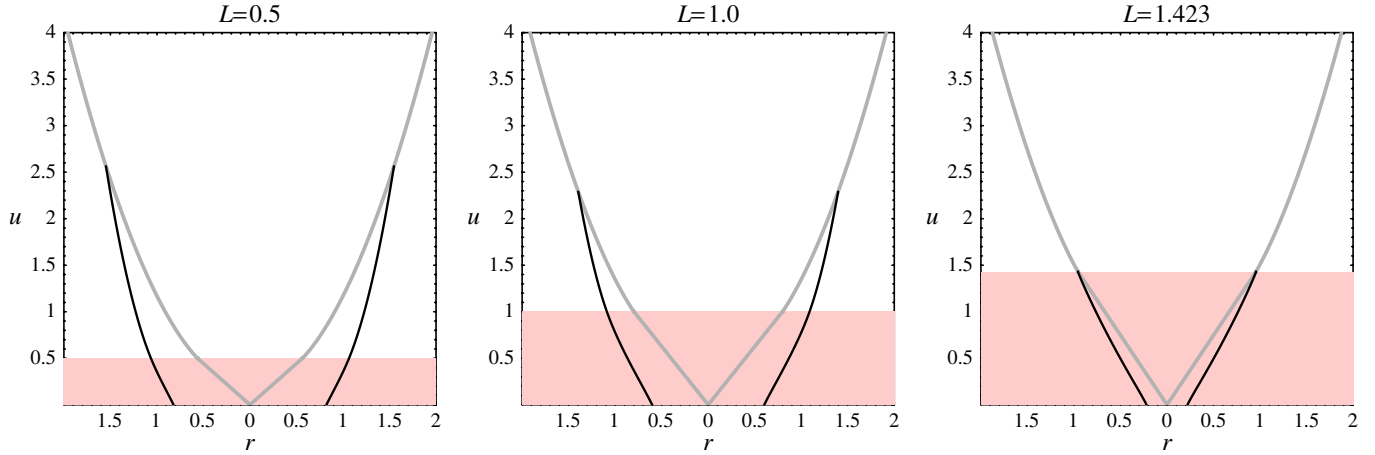


FIG. 7 (color online). The top views of the AH in case (0) for $L = 0.5, 1.0,$ and 1.423 . For all $0 \leq L \leq 1.423$, we find only one solution. At $L = 1.423$, the AH almost touches the energy source at the symmetry axis. No AH exists for $L \geq 1.424$.

distributes at $0 \leq \bar{u} \leq L$ on the symmetry axis. For $L \geq 1.424$, we found no solution. Thus, on the slice we studied, the condition of AH formation is given by $L \leq 1.423$ in the length unit $r_h(2p) = 1$.

B. Collision of a spinning gyraton with an AS particle

Next we show the results of cases (1a) and (1b), i.e., the collisions of spinning a - and b -gyratons with an AS particle.

Figure 8 shows the AHs in case (1a) for parameters $L = 0.1$ and $j = 0.05, 0.10,$ and 0.1466 . We found two solutions to the AH equation, which correspond to the AH and the inner boundary of the trapped region. As the value of j is increased for a fixed value of L , the trapped region grows smaller and the two solutions coincide at some value of $j =$

j_{crit} . The trapped region vanishes for $j \geq j_{\text{crit}}$. The similar phenomena was observed also in case (1b). In Fig. 9, the AH shape in case (1b) is shown for the same parameters as those in Fig. 8. Again, there are two solutions and they degenerate at some critical value $j = j_{\text{crit}}$.

As it has been found above, the spin makes the formation of the AH more “difficult.” This is because the gravitational field generated by the spin source is repulsive as we pointed out in Sec. II. As the value of j is increased, the repulsive force surpasses the attractive force generated by the energy source and causes the extinction of the AH.

We studied the value of j_{crit} as a function of L , i.e., $j_{\text{crit}}(L)$. In Fig. 10, the critical lines for the AH formation in the (L, j) -plane are shown for both cases. The AH formation is allowed under the critical line. For $L \lesssim 1$, the two

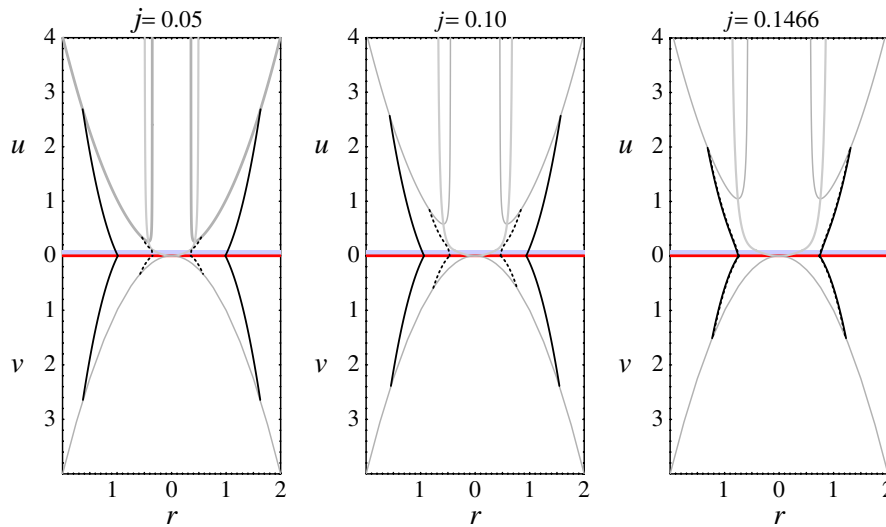


FIG. 8 (color online). The top views of the AH in case (1a) for $L = 0.1$ and $j = 0.05, 0.10,$ and $j_{\text{crit}} = 0.1466$. For all $0 < j \leq 1.466$, there are the AH (solid lines) and the inner boundary of the trapped region (dashed lines). The trapped region shrinks as j is increased and no AH exists for $j \geq 0.1467$.

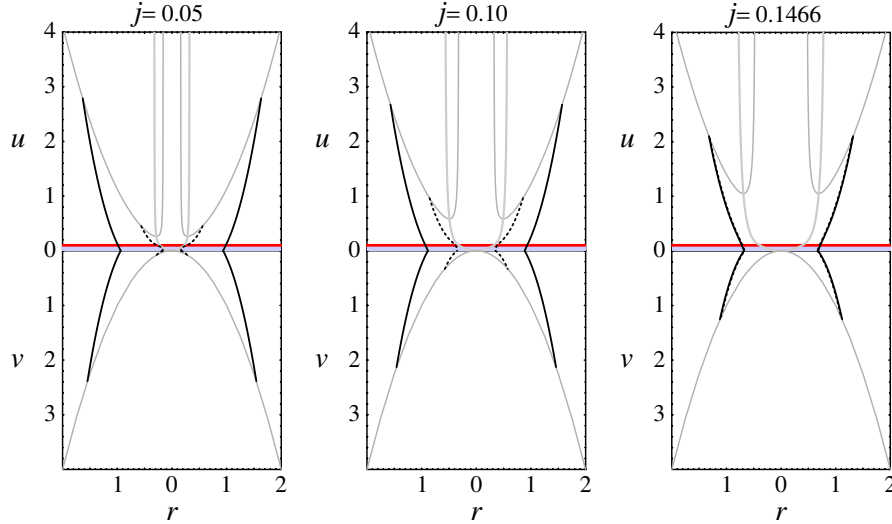


FIG. 9 (color online). The same as Fig. 8 but for case (1b). For $L = 0.1$, the critical value of AH formation j_{crit} is almost the same as that in case (1a).

critical lines agree well and go to zero in the limit $L \rightarrow 0$. Both critical lines have the peak $j \approx 0.24$ at $L \approx 0.6$. For $L \geq 1$, the two critical lines show different behaviors. In case (1a), $j_{\text{crit}}(L)$ decreases and becomes zero at $L = e := \exp(1)$. On the other hand, it decays (almost) exponentially but never becomes zero in case (1b).

Let us discuss the reasoning for these results. The reason why j_{crit} goes to zero in the limit $L \rightarrow 0$ is as follows. As stated above, the extinction of the AH is caused by the repulsive force generated by the spin source. Thus, it is useful to introduce a radius r_{eq} where the attractive force due to the energy and the repulsive force due to the spin balance one another. For this purpose, let us recall Figs. 3 and 4 that show the propagation of light rays through the

gravitational field of the gyratons. The figures indicate the existence of r_{eq} such that the rays with $r > r_{\text{eq}}$ shrink and those with $r < r_{\text{eq}}$ expand in the region $\bar{u} > L$. Such r_{eq} is found by the equation $G_{,u}(L, r_{\text{eq}}) = 0$ and solved as

$$r_{\text{eq}} = \begin{cases} \sqrt{L + j^2/L}, & a\text{-gyraton}, \\ \sqrt{j^2/L}, & b\text{-gyraton}. \end{cases} \quad (53)$$

As L is decreased, r_{eq} becomes larger, which indicates that the repulsive force becomes stronger. It is natural that $r_{\text{eq}} \leq 1$ represents the condition for AH formation, and it is reduced to $j^2 \leq L$ in the limit $L \rightarrow 0$. This explains the behavior of the critical lines at $L \ll 1$.

At $L \geq 1$, the condition $r_{\text{eq}} \leq 1$ does not explain the numerical results well. This is because the above discussion takes account only of the gravitational structure in the transverse direction of motion, which would be sufficient in the case $L \ll 1$, while the spin duration L plays an important role for the AH existence in the case $L \geq 1$. Let us first consider case (1a). Taking a limit $j \rightarrow 0$ for $L \geq 1$, the AH solution is expected to reduce to that for the collision of two AS particles:

$$h^{(1)}(r) = h^{(2)}(r) = 2r^2 \log r, \quad (54)$$

with $r_{\text{min}} = 1$ and $r_{\text{max}} = \sqrt{e}$. This statement holds only for $L < e$. In the case $L > e$, the ‘‘solution’’ (54) plunges into the crossing singularity. In other words, it crosses the spin source distributed on the symmetry axis for $0 \leq u \leq L$, on which the outer boundary condition cannot be imposed. Thus in case (1a), the situations $j = 0$ and $j = 0_+$ are different. This is the reason why the critical line intersects the L -axis at $L = e$.

Next we discuss case (1b). In the limit $j \rightarrow 0$ for $L \geq 1$, the AH solution reduces to

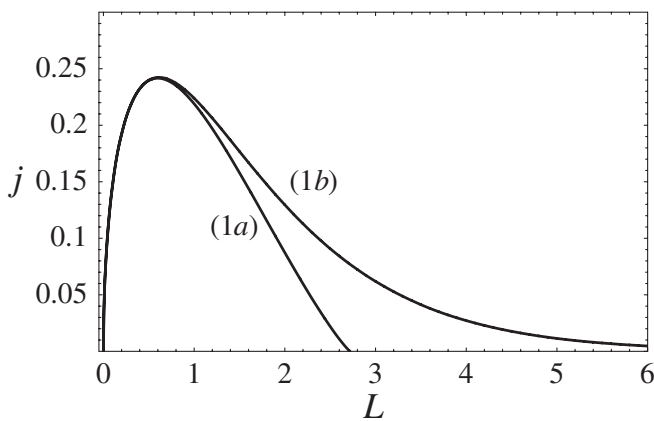


FIG. 10. The critical line on the (L, j) -plane for AH formation in cases (1a) and (1b). The AH formation is allowed under the critical line. The two critical lines almost coincide for $L \leq 1$ and go to zero in the limit $L \rightarrow 0$. The critical line of the (1a) case intersects the L -axis at $L = e$, while that of the (1b) case becomes exponentially close to the L -axis as L is increased.

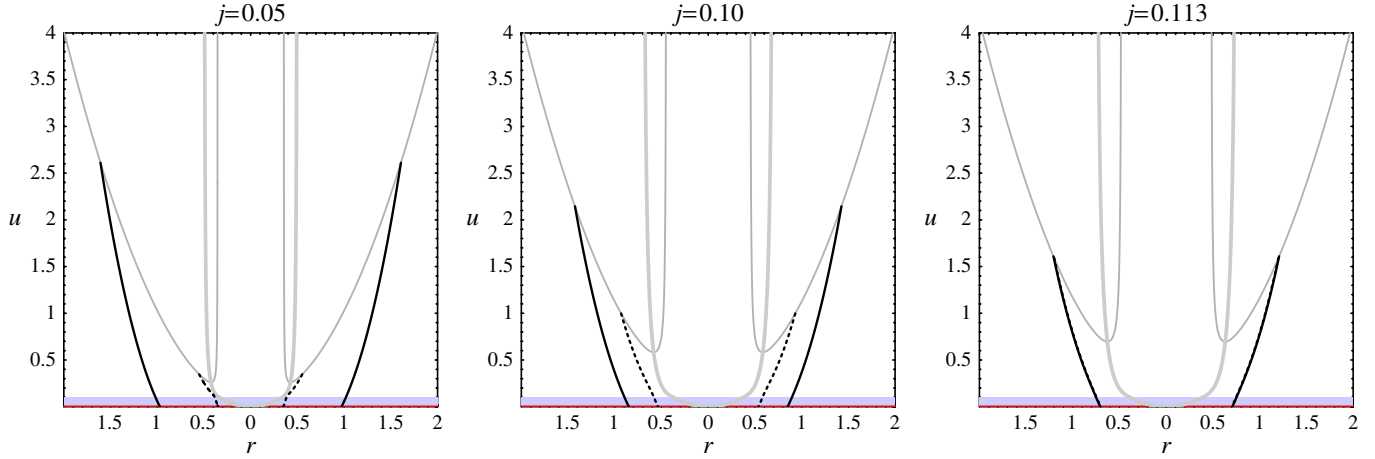


FIG. 11 (color online). The top views of the AH (solid lines) and the inner boundary of the trapped region (dashed lines) in case (2a) for $L = 0.1$ and $j = 0.05, 0.10,$ and 0.113 . No AH exists for $j \geq 0.113$.

$$h^{(1)}(r) = \begin{cases} 2r^2 \log r + L, & (1 \leq r \leq \sqrt{e}), \\ 2 \log(r/r_{\min}), & (r_{\min} \leq r \leq 1), \end{cases} \quad (55)$$

$$h^{(2)}(r) = 2r^2 \log(r/r_{\min}), \quad (r_{\min} \leq r \leq \sqrt{e}r_{\min}), \quad (56)$$

where $r_{\min} = e^{-L/2}$. In contrast to the (1a) case, this statement is valid for arbitrary L , because the AH never touches the spin source. Then, the condition for AH formation in the case $j > 0$ is expected to be $r_{\min} \geq r_{\text{eq}}$, which is equivalent to $j^2 \leq Le^{-L}$. This explains the exponential decay of the critical line in the (1b) case.

Note that the above interpretations, especially the ones for $L \geq 1$, strongly depend on the slice we have adopted. Thus there is no reason why the above discussion holds for another slice that is future to our slice. Hence, we should keep in mind the possibility that the critical line does not touch the L -axis in another slice also in case (1a).

To summarize, for the collision of a spinning gyraton with the AS-gyraton and for the slice we have adopted, the

condition for the AH formation is roughly expressed as $L \sim 1$ and $j \leq 0.25$ in both cases.

C. Collision of two spinning gyratons

Finally we show the results of cases (2a) and (2b), i.e., the collisions of two spinning a - and b -gyratons (identical up to helicities).

Figure 11 shows the AHs in case (2a) for parameters $L = 0.1$ and $j = 0.05, 0.10,$ and 0.113 . Similarly to the (1a) case, there are two solutions to the AH equation, which surround the trapped region, and they coincide at some value of $j = j_{\text{crit}}$ as the value of j is increased for a fixed value of L . The similar phenomena was observed also in case (2b). In Fig. 12, the AH shape in case (2b) is shown for $L = 0.1$ and $j = 0.01, 0.05,$ and 0.0981 . Again, we found two solutions and their disappearance at some critical value $j = j_{\text{crit}}$. Similarly to cases (1a) and (1b), the spin has the effect to make the AH formation more difficult.

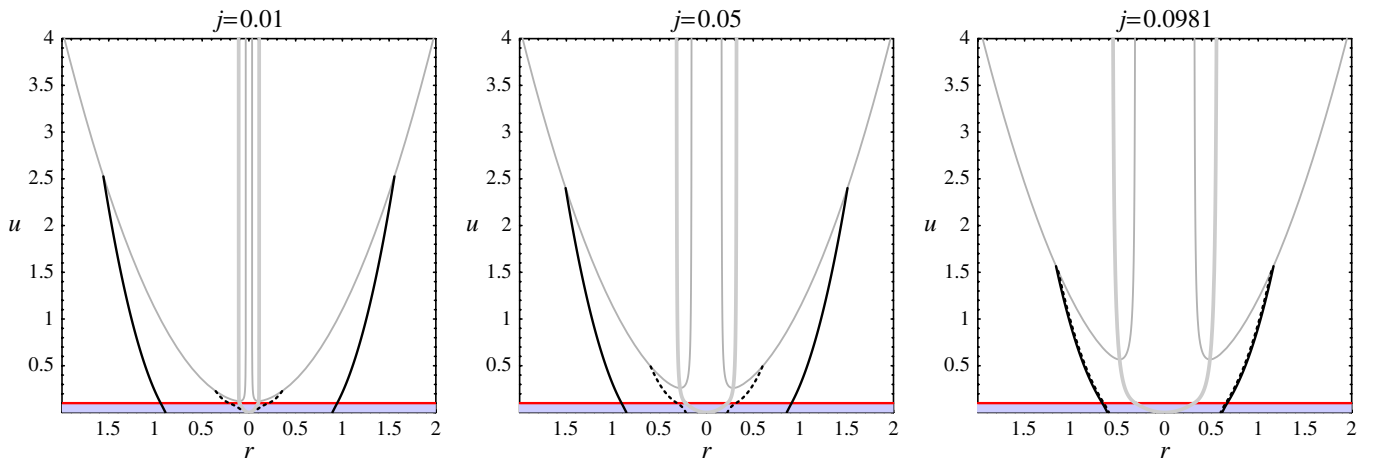


FIG. 12 (color online). The top views of the AH (solid lines) and the inner boundary of the trapped region (dashed lines) in case (2b) for $L = 0.1$ and $j = 0.01, 0.05,$ and 0.0981 . No AH exists for $j \geq 0.0982$.

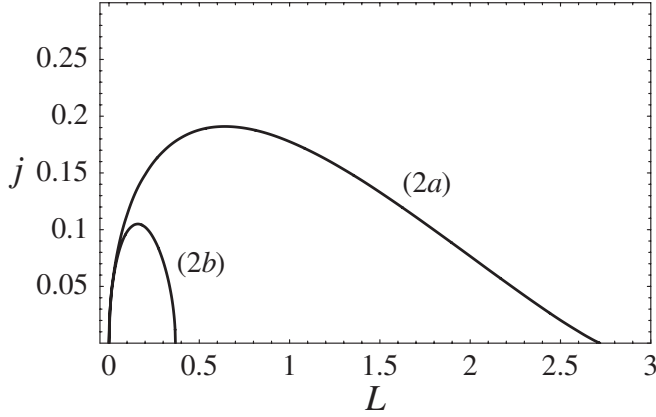


FIG. 13. The critical lines on the (L, j) -plane for AH formation in cases (2a) and (2b). The two lines go to zero in the limit $L \rightarrow 0$. The critical lines of the (2a) and (2b) cases intersect the L -axis at $L = e$ and $1/e$, respectively.

We studied the value of j_{crit} as a function of L . In Fig. 13, the critical line for cases (2a) and (2b) in the (L, j) -plane is shown. The AH formation is allowed under each critical line.

Let us first discuss the critical line of the (2a) case. It goes to zero in the limit $L \rightarrow 0$ and intersects the L -axis at $L = e$. It has a peak $j \approx 0.19$ at $L \approx 0.6$, and this peak value is somewhat smaller than the peak value 0.24 of the (1a) case. Hence, the critical line of the (2a) case has the same features as that of the (1a) case except that the peak value is smaller. For the behaviors at $L \rightarrow 0$ and $L \rightarrow e$, the same reasoning to the results of the (1a) case holds. Compared to the (1a) case, the AH formation is expected to become more difficult, since both gyratons have the repulsive forces around their centers in the (2a) case while only one gyration has the repulsive force in the (1a) case. This leads to the smaller peak value of $j_{\text{crit}}(L)$ in the (2a) case.

Now we discuss the critical line of the (2b) case. It goes to zero in the limit $L \rightarrow 0$ with the same reason to the (1b) case. It has a peak $j \approx 0.105$ at $L \approx 0.16$, and intersects the L -axis at $L = 1/e$. The allowed region of the (2b) case is much smaller than that of the (2a) case. The condition of the AH formation strongly depends on the relative locations of the energy and spin profiles. The reason can be understood as follows. In the limit $j \rightarrow 0$, the AH becomes

$$h(r) = \begin{cases} 2r^2 \log(r/\sqrt{r_{\min}}) + L, & (\sqrt{r_{\min}} \leq r \leq \sqrt{er_{\min}}), \\ 2r_{\min} \log(r/r_{\min}), & (r_{\min} \leq r \leq \sqrt{r_{\min}}), \end{cases} \quad (57)$$

where r_{\min} is given by the equation

$$L = -r_{\min} \log r_{\min}. \quad (58)$$

This equation has two solutions for $0 \leq L < 1/e$, one degenerate solution for $L = 1/e$, and no solution for $L > 1/e$. Thus the AH formation in the $j \rightarrow 0$ limit is allowed only for $0 \leq L \leq 1/e$. This is the reason why the allowed region is restricted to $0 \leq L \leq 1/e$ and is much smaller than that of case (2a). However, we should keep in mind that this discussion is specific to the slice we have adopted. In the case $j = 0$, the AH formation is allowed on a slice appropriately taken at the future to our slice. Hence, the allowed region in the (2b) case is so small because of the artificial effect of the slice choice. In the next section, we demonstrate that this expectation is true by solving a part of the spacetime after the collision using the method of perturbation.

To briefly summarize, for the collision of two spinning gyratons, the condition of the AH formation on the slice we have adopted is roughly expressed as $L \sim 1$ and $j \lesssim 0.2$ in the (2a) case, while $L \sim 0.15$ and $j \lesssim 0.1$ in the (2b) case.

V. SECOND-ORDER EVOLUTION

In a general case, finding the spacetime structure after the collision of two gyratons requires numerical simulations. However, in the (2b) case, we can go a little bit further using the method of perturbation assuming that the spins of incoming gyratons are small.

Figure 14 shows the schematic spacetime structure in the (2b) case where the gyration 1 with the spin j and the gyration 2 with the spin σj collide. (Here $\sigma = \pm 1$, but we note that the solution to the Einstein equations found in the Sec. VA can be applied to an arbitrary value of σ .) For $\sigma > 0$ the two spins have the same direction (i.e., the helicities of incoming gyratons have opposite signs), while for $\sigma < 0$ the two spins have opposite directions (i.e., the helicities of incoming gyratons have the same sign). The exact metrics in regions I, IIA, IIB, IIIA, and IIIB are known. We focus our attention on finding the metric in region IVA ($0 \leq u \leq L$ and $0 \leq v \leq L$), where the gravitational spin-spin interaction begins. If the value of j is small, we can expand the metric in terms of j . The background spacetime is the Minkowski spacetime, because regions I, IIA, and IIIA are flat for $j = 0$. The first-order perturbation is easily solved. Because the metric in regions IIA and IIIA is

$$ds^2 = \begin{cases} -dudv + dr^2 + r^2 d\phi^2 + 2\epsilon(u/r) dr d\phi, & \text{region IIA,} \\ -dudv + dr^2 + r^2 d\phi^2 + 2\epsilon(\sigma v/r) dr d\phi, & \text{region IIIA,} \end{cases} \quad (59)$$

where

$$\epsilon = 2j/L, \quad (60)$$

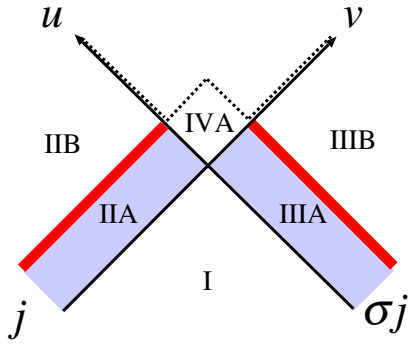


FIG. 14 (color online). Schematic spacetime structure of the gyraton collision in the (2b) case. Region IVA can be solved using a perturbative method, assuming the spins are small. Then we study the AH on the new slice shown by a dotted line, which is the future edge of the solved region.

the metric in region IVA is found to be

$$ds^2 = -dudv + dr^2 + r^2 d\phi^2 + 2\epsilon \frac{u + \sigma v}{r} dr d\phi, \quad (61)$$

using the linearity of the first-order perturbation. Strictly speaking, we have to specify the properties of matter interaction between the sources of two incoming gyrators in order to determine the metric of the whole region IVA. The domain where the matter interaction is important is within the light cone of the source collision, i.e. $uv > r^2$. The spacetime structure of the other domain $uv < r^2$ in region IVA is not affected by the matter interaction and therefore the metric (61) can be applied for this domain. In the following, we restrict our attention to the domain $uv < r^2$ and do not consider the effect of matter interaction.

In order to study the condition of AH formation, the above first-order solution is not sufficient because the nonexistence of the AH is due to the effect of nonlinear terms in j . Thus we should study (at least) the second-order perturbation, with which we will proceed in this section.

This study has the following meanings. First, it will clarify to what extent the condition of AH formation depends on the choice of the slice. In the previous section, we found that the conditions are very different in the (2a) and (2b) cases. Although we expected that this is due to the artificial effect of the slice choice, the study in this section will explicitly show whether such an expectation is correct or not. Next, by comparing the two cases $\sigma = \pm 1$, we can study the properties of the gravitational field generated by the spin-spin interaction in the gyraton collision. As a result, we will find the dependence of the AH formation on the relative helicities of the incoming gyrators. For the old slice $u \geq 0 = v$ and $v \geq 0 = u$, we found no difference between $\sigma = \pm 1$ cases because the function $G(u, r)$ on the chosen slice depends only on j^2 . However, the second-order structure of region IVA will depend also on σ and it will lead to different conditions for the AH formation on the new slice, which consists of the future

boundaries of regions IVA, IIB, and IIIB as illustrated in Fig. 14.

The gravitational spin-spin interactions were studied for a spinning test particle around a rotating body [23], for a massless particle passing by a rotating body [24,25], and for binary systems of weakly gravitating bodies [26,27]. In the case of binary systems, the contribution of spin-spin interaction to the relative acceleration, \vec{a}_{SS} , between two bodies was calculated as

$$\vec{a}_{SS} = -\frac{3}{\mu r^4} [\vec{n}(\vec{S}_1 \cdot \vec{S}_2) + \vec{S}_1(\vec{n} \cdot \vec{S}_2) + \vec{S}_2(\vec{n} \cdot \vec{S}_1) - 5\vec{n}(\vec{n} \cdot \vec{S}_1)(\vec{n} \cdot \vec{S}_2)], \quad (62)$$

where \vec{r} is a relative location $\vec{r} = \vec{r}_1 - \vec{r}_2$, $\vec{n} := \vec{r}/r$, μ is the reduced mass, \vec{S}_1 and \vec{S}_2 are spins of two bodies. For $\vec{S}_1 = S_1 \vec{n}$ and $\vec{S}_2 = S_2 \vec{n}$, the spin-spin acceleration becomes $\vec{a}_{SS} = (6/\mu r^4) S_1 S_2 \vec{n}$. Therefore, for a binary with both spins aligned with the relative location vector \vec{r} (i.e., both S_1 and S_2 are positive), the spin-spin interaction is repulsive. Another example where the spin-spin interaction plays an important role is the Hawking emission of massless particles with spin (e.g., photons and neutrinos) by a Kerr black hole. In this process, the flux of particles with a given helicity created by the rotating black hole has anisotropic distribution. The black hole radiates more particles in the direction where the spin is aligned to the angular momentum of the black hole than in the opposite direction ([28–30] and see also [31] for higher-dimensional cases). This indicates the existence of a spin-spin interaction between the black hole and an emitted particle, which is repulsive when two spins have the same direction. If we assume that a spin-spin interaction similar to the above examples is present for a system of two relativistic spin particles, the black hole formation in the head-on collision of two gyrators with the same spin direction ($\sigma = +1$) is expected to be more difficult than that with the opposite spin directions ($\sigma = -1$). The calculations in this section will confirm this.

In Sec. VA, we derive the second-order Einstein equations and solve them. Then the AH equation and the boundary condition on the new slice is studied in Sec. VB. We present the numerical results in Sec. VC. In Sec. VD, we discuss the properties of the gravitational field in region IVA in more detail using the null geodesics. This helps us to interpret the results of AH formation.

A. Second-order equations

We adopt $\epsilon = 2(j/L)$ as a small expansion parameter and assume the following metric ansatz in (u, v, r, ϕ) coordinates:

$$ds^2 = -(1 + \epsilon^2 c) dudv + (1 + \epsilon^2 a) dr^2 + r^2 (1 + \epsilon^2 b) d\phi^2 + 2\epsilon \frac{u + \sigma v}{r} dr d\phi. \quad (63)$$

Here a , b , and c are functions of u , v , and r . Expanding the Einstein equations up to the second order in ϵ , we obtain:²

$$a_{,uu} + b_{,uu} = \frac{1}{r^4}, \quad (64)$$

$$a_{,vv} + b_{,vv} = \frac{\sigma^2}{r^4}, \quad (65)$$

$$2c_{,uv} - \frac{1}{2} \left(c_{,rr} + \frac{c_{,r}}{r} \right) + a_{,uv} + b_{,uv} = \frac{\sigma}{r^4}, \quad (66)$$

$$c_{,ur} + b_{,ur} + \frac{b_{,u}}{r} = \frac{a_{,u}}{r} - \frac{2}{r^5} (u + \sigma v), \quad (67)$$

$$c_{,vr} + b_{,vr} + \frac{b_{,v}}{r} = \frac{a_{,v}}{r} - \frac{2\sigma}{r^5} (u + \sigma v), \quad (68)$$

$$2c_{,rr} - 4a_{,uv} + b_{,rr} + \frac{2}{r} b_{,r} = \frac{a_{,r}}{r} + \frac{4}{r^6} (u + \sigma v)^2 - \frac{4\sigma}{r^4}, \quad (69)$$

$$2\frac{c_{,r}}{r} - 4b_{,uv} + b_{,rr} + \frac{2}{r} b_{,r} = \frac{a_{,r}}{r} + \frac{4}{r^6} (u + \sigma v)^2 - \frac{4\sigma}{r^4}. \quad (70)$$

These relations follow from uu , vv , uv , ur , vr , rr , $\phi\phi$ components of the equation $R_{\mu\nu} = 0$, respectively. The other components vanish automatically.

The initial conditions for this system are found by expanding the exact metric in regions IIA and IIIA in terms of j :

$$a = b = \frac{u^2}{4r^4}, \quad c = 0, \quad \text{for } v = 0, \quad (71)$$

$$a = b = \frac{\sigma^2 v^2}{4r^4}, \quad c = 0, \quad \text{for } u = 0. \quad (72)$$

The solutions satisfying these initial conditions are found as

$$a = \frac{1}{4r^4} (u + \sigma v)^2 + \frac{\sigma}{2r^2} \left[x \left(3 - \frac{1}{1-x} \right) + \log(1-x) \right], \quad (73)$$

$$b = \frac{1}{4r^4} (u + \sigma v)^2 - \frac{\sigma}{2r^2} \left[x \left(1 - \frac{1}{1-x} \right) + \log(1-x) \right], \quad (74)$$

²More strictly, we should put $g_{r\phi} = \epsilon[u\theta(u) + \sigma v\theta(v)]/r$ in Eq. (63), although we do not show this because the equations become tedious. We note that this step function formula leads to the junction conditions at $u = 0 \leq v \leq L$ and $v = 0 \leq u \leq L$ through $R_{uu} = R_{vv} = 0$, which the solution (73)–(75) satisfies.

$$c = -\frac{\sigma}{2r^2} \frac{x}{1-x}, \quad (75)$$

with

$$x = uv/r^2. \quad (76)$$

We discuss now the properties of the second-order solution in region IVA. First, a line u , r , $\phi = \text{const}$ is a null geodesic, although when $c \neq 0$ the coordinate v is no longer an affine parameter along the geodesic. Similarly a line v , r , $\phi = \text{const}$ is a null geodesic, although the coordinate u is not an affine parameter along it. Thus, the coordinates (u, v, r, ϕ) simultaneously label the two null geodesic congruences.

Next, all second-order quantities a , b , and c diverge at $x = 1$, i.e., $uv = r^2$. Therefore it is interesting to ask whether $x = 1$ is a physical singularity or a coordinate singularity. For this purpose, we calculated the leading term in the expansion of the Kretschman invariant $K := R_{abcd}R^{abcd}$ near this point:

$$K = \epsilon^4 \sigma^2 \frac{4(3-x)}{r^8(1-x)^3}. \quad (77)$$

Evidently it is divergent at $x = 1$. Because we are studying perturbation, the formula (77) cannot be trusted in the neighborhood of $x = 1$, and we cannot definitely claim that there is a physical singularity at $x = 1$. Still, Eq. (77) indicates that there always exists the region where the perturbation breaks down around $x = 1$ for any small j . Hence, it is natural to expect that the exact solution, if it is found, also will have a real singularity of which location is shifted by $O(j^2)$ from $x = 1$. If this is the case, a physical singularity is produced at $u = v = r = 0$ by the collision of gyratons and expands (almost) at the speed of light because $uv = r^2$ represents a light cone in the background spacetime. We note that this singularity formation is a consequence of the infinitely narrow shape of the source, i.e. Eqs. (3) and (4). In a realistic case where each source has a finite radius $\bar{r} = \bar{r}_s$, the metric is regular at the source and therefore the singularity is not produced at $uv = r^2$. Then the spacetime structure in the region $uv > r^2$ is determined by matter interaction between the two sources. Although the dependence on the properties of matter interaction is an interesting issue, it is not tractable by the perturbation.

Finally, although the metric is continuous everywhere, first derivatives of a , b , and c are discontinuous at $u = 0 \leq v \leq L$ and $v = 0 \leq u \leq L$. As a result, some components of Riemann curvature, R_{urur} , R_{vrvr} , $R_{u\phi u\phi}$, and $R_{v\phi v\phi}$, have the delta function singularity there:

$$R_{urur} = \epsilon^2 \frac{\sigma}{4r^4} \left[\frac{v^2(3-x)}{r^2(1-x)} \theta(u) - 2v\delta(u) \right] \theta(v), \quad (78)$$

$$R_{u\phi u\phi} = \epsilon^2 \frac{\sigma}{4r^4} \left[\frac{v^2(3-x)}{r^2(1-x)} \theta(u) + 2v\delta(u) \right] \theta(v), \quad (79)$$

and R_{vrvr} and $R_{v\phi v\phi}$ are obtained by changing u and v in Eqs. (78) and (79), respectively (but note that the Ricci tensor is zero in the sense of distribution). Hence, at the encounter of the two spin flows, a new shock field is produced and it grows linearly in u or v . The above four components of Riemann curvature are proportional to σ and thus the feature of the shock gravitational field at $u = 0 \leq v \leq L$ and $v = 0 \leq u \leq L$ depends on the sign of σ .

B. AH equation on the new slice

Because the metric in region IVA has properties that are somewhat different from other regions, we should derive the AH equation on the new slice. But the basic idea is the same as that in Sec. II.

The second-order metric can be written like

$$ds^2 = -C dudv + Adr^2 + B(d\phi + Ddr)^2, \quad (80)$$

where A , B , C , and D are functions of u , v , and r . In region IVA,

$$\begin{aligned} A &= 1 + \epsilon^2 \left[a - \frac{(u + \sigma v)^2}{r^4} \right], & B &= r^2(1 + \epsilon^2 b), \\ C &= 1 + \epsilon^2 c, & D &= \epsilon \frac{(u + \sigma v)}{r^3}, \end{aligned} \quad (81)$$

and in region IIB,

$$\begin{aligned} A &= \left(1 + \frac{u_L}{r^2}\right) \left\{ 1 + \frac{u_L}{r^2} - \frac{j^2}{r^2} \left[3 + \left(\frac{5}{r^2} + \frac{6}{L}\right) u_L \right] \right\}, \\ B &= \left(r - \frac{u_L}{r}\right) \left\{ r - \frac{u_L}{r} + \frac{j^2}{r^3} \left[1 + \left(\frac{1}{r^2} + \frac{2}{L}\right) u_L \right] \right\}, \\ C &= 1, & D &= \frac{2j}{r^3}, \end{aligned} \quad (82)$$

where $u_L := u - L$ and we have kept terms up to second order in j . Based on this metric, we solve the AH equation on the new slice as shown in Fig. 15. The new slice consists of four parts: (1) $v = 0$, $L \leq u$; (2) $u = L$, $0 \leq v \leq L$;

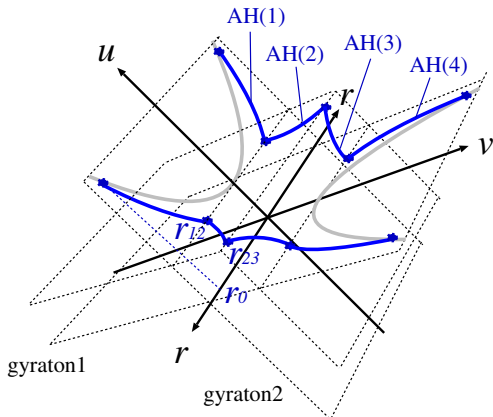


FIG. 15 (color online). The new slice on which we study the AH formation and the schematic shape of AH in the new slice.

(3) $v = L$, $0 \leq u \leq L$; (4) $u = 0$, $L \leq v$. Correspondingly, the AH consists of $u = h^{(1)}(r)$ on slice (1); $v = h^{(2)}(r)$ on slice (2); $u = h^{(3)}(r)$ on slice (3); $v = h^{(4)}(r)$ on slice (4).

We consider the AH equation for $h(r) := h^{(2)}(r)$. The tangent vector of the null geodesic congruence from the surface is given by

$$(k^u, k^v, k^r, k^\phi) = \left(2, \frac{C}{2A} h_{,r}^2, \frac{C}{A} h_{,r}, -\frac{CD}{A} h_{,r} \right). \quad (83)$$

and the condition of zero expansion becomes

$$\partial_r k^r + \frac{A_{,u} k^u + A_{,v} k^v + A_{,r} k^r}{2A} + \frac{B_{,u} k^u + B_{,v} k^v + B_{,r} k^r}{2B} = 0, \quad (84)$$

or equivalently

$$\begin{aligned} h_{,rr} + \left(-3 \frac{A_{,v}}{A} + \frac{B_{,v}}{B} + 4 \frac{C_{,v}}{C} \right) \frac{h_{,r}^2}{4} + \left(-\frac{A_{,r}}{A} + \frac{B_{,r}}{B} + 2 \frac{C_{,r}}{C} \right) \\ \times \frac{h_{,r}}{2} + \frac{A}{C} \left(\frac{A_{,u}}{A} + \frac{B_{,u}}{B} \right) = 0. \end{aligned} \quad (85)$$

The equation for $h^{(1)}(r)$ is obtained by just changing u and v in Eq. (85).

Now we explain the boundary conditions. At the intersection of the AH and the coordinate singularity $u = L + r^2$, we impose

$$h_{,r}^{(1)} = -2B_{,r}/B_{,u}. \quad (86)$$

with the same reason as that in Sec. II. At the intersection of slices (1) and (2), we impose the condition that two null vectors of both sides of the surface be parallel, which is equivalent to

$$h_{,r}^{(1)} h_{,r}^{(2)} = 4A, \quad (87)$$

where we used $C = 1$ on $v = 0$. Similarly, at the intersection of slices (2) and (3), we impose

$$h_{,r}^{(2)} h_{,r}^{(3)} = 4A/C. \quad (88)$$

In the cases $\sigma = \pm 1$, the functions A , B , and C are symmetric with respect to u and v . Because D does not appear in the AH equation and the boundary conditions, the AH shape is symmetric with respect to the plane $u = v$. Hence, we only have to study $h^{(1)}(r)$ and $h^{(2)}(r)$, and the boundary condition (88) is reduced to

$$h_{,r}^{(2)} = 2\sqrt{A/C}. \quad (89)$$

We also note that, because the functions A , B , and C do not depend on the sign of j , the condition for the AH formation is written in terms of $|j|$ and L for each σ . For this reason, j is assumed to be positive without loss of generality in the following.

The numerical procedure is as follows. First, we choose some value of r_0 and start solving $h^{(1)}(r)$ with the boundary

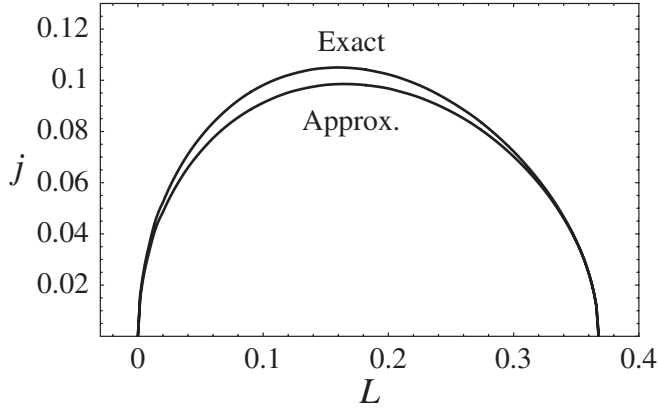


FIG. 16. The critical lines for AH formation on the (L, j) -plane for the old slice. The results obtained by the exact formula and by the second-order approximation (denoted by “Exact” and “Approx.,” respectively) are compared. The two results agree well and the error is $O(j^2)$.

condition $h^{(1)}(r_0) = L + r_0^2$ and (86). When $h^{(1)}(r)$ becomes L at $r = r_{12}$, we solve $h^{(2)}$ using the boundary conditions $h^{(2)}(r_{12}) = 0$ and $h_{,r}^{(2)} = 4A/h_{,r}^{(1)}$. When $h^{(2)}$ becomes L at $r = r_{23}$, we check whether the boundary condition (89) is satisfied. Iterating these steps for various values of r_0 , we can judge the existence of the AH and find its location.

C. Numerical results

In order to test the reliability of the second-order approximation, we studied the condition of AH existence on the old slice $u \geq 0 = v$ and $v \geq 0 = u$ using the exact formula and the second-order formula for $G(u, r)$ and compared the two results. Figure 16 shows the regions of AH formation on the (L, j) -plane obtained by the two methods. The two results agree well and the difference is $O(j^2)$. This demonstrates the reliability of the second-order

approximation for the old slice. Later, we will discuss also the reliability of the approximation for the AH study on the new slice.

Now we show the results of the new slice. We first show the case $\sigma = +1$ where the spins of two gyratons have the same direction (i.e., the helicity of one gyration is positive and that of the other is negative). Figure 17 shows top views of the AH shape for $L = 0.3$ and $j = 0.05, 0.1$, and 0.1129 . We could not find the solution for $j \geq 0.1130$. Similarly to the case of the old slice, there is some critical value of the spin $j_{\text{crit}}^{(+)}(L)$ for the AH formation. There are two solutions for each $j < j_{\text{crit}}^{(+)}(L)$, which correspond to the AH and the inner boundary of the trapped region, and they coincide at $j = j_{\text{crit}}^{(+)}(L)$.

Next we show the case $\sigma = -1$, where the spins of two gyratons are oppositely directed (i.e., the helicities of gyratons are both positive or negative). Figure 18 shows top views of the AH shape for $L = 0.3$ and $j = 0.1, 0.15, 0.1581$. For $j \leq 0.1$, only one solution is found. Hence, there is an AH but no inner boundary of the trapped region. For $0.15 \leq j \leq 0.1581$, two solutions are found for each j . Thus, the inner boundary of the trapped region appears for these values of j . For $j \geq 0.1582$, there was no solution. The critical value $j_{\text{crit}}^{(-)}(L)$ of AH formation for $\sigma = -1$ is larger than $j_{\text{crit}}^{(+)}(L)$. Thus in the case $\sigma = -1$, the AH is allowed to form in a larger parameter regime compared to the case $\sigma = +1$.

We studied the critical value $j_{\text{crit}}^{(\sigma)}(L)$ as functions of L for the cases $\sigma = \pm 1$. Before showing the obtained results, we comment on the reliability of the second-order approximation. In order to evaluate the error, we checked the maximum values of $\epsilon^2 a$, $\epsilon^2 b$, and $\epsilon^2 c$ on the AH at the critical line. In the case $\sigma = +1$, $\max[\epsilon^2 a] \leq 0.32$, $\max[\epsilon^2 b] \leq 0.20$, and $\max[\epsilon^2 c] \leq 0.14$ are satisfied for arbitrary L . Therefore the expected error is about 20%. In the case $\sigma = -1$, they are found to be $\max[\epsilon^2 a] \approx 0.38$,

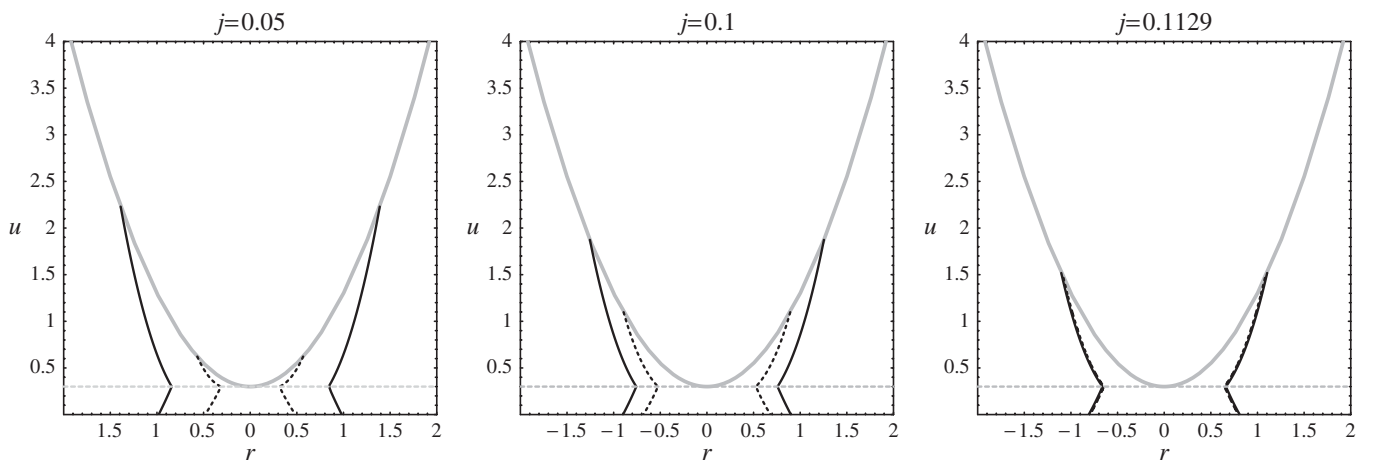


FIG. 17. The top view of the AH (solid lines) and the inner boundary of the trapped region (dashed lines) in the case $\sigma = +1$ for $L = 0.3$ and $j = 0.05, 0.1$, and 0.1129 .

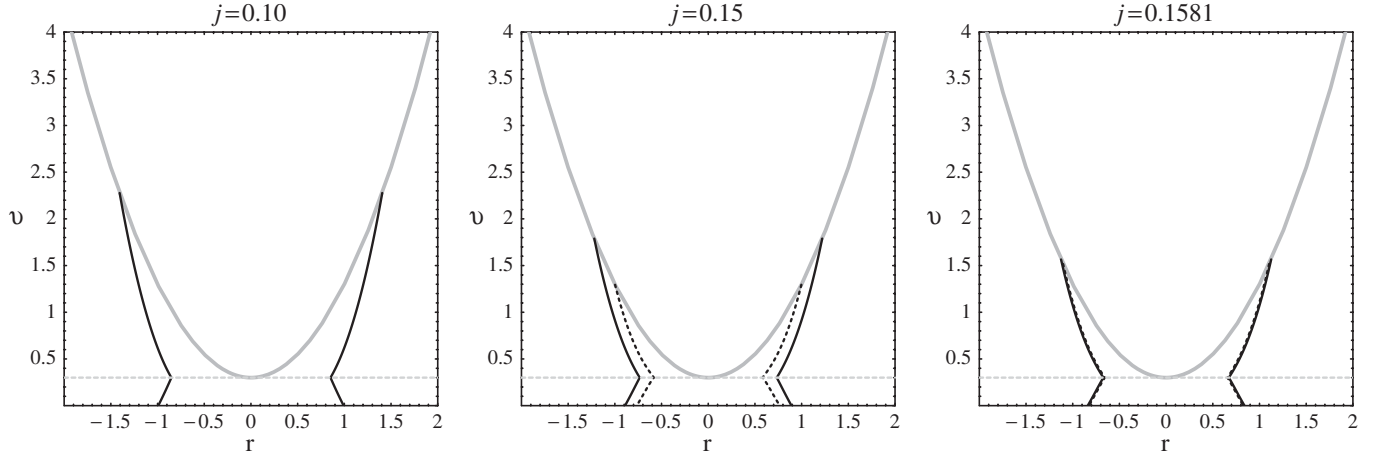


FIG. 18. The top view of the AH (solid lines) and the inner boundary of the trapped region (dashed lines) in the case $\sigma = -1$ for $L = 0.3$ and $j = 0.1, 0.15,$ and 0.1581 . For $j = 0.1$, there is no inner boundary of the trapped region.

$\max[\epsilon^2 b] \approx 0.13$, and $\max[\epsilon^2 c] \approx 0.12$ for $L \lesssim 0.3$, and thus the expected error is about 30% for $L \lesssim 0.3$. However, for $L = 1.0$, their values grow large: $\max[\epsilon^2 a] \approx 0.96$, $\max[\epsilon^2 b] \approx 0.97$, and $\max[\epsilon^2 c] \approx 0.95$, and the approximation obviously breaks down at $L \gtrsim 0.9$. Thus unfortunately we cannot trust the shape of the critical line for $L \gtrsim 0.9$ in the case $\sigma = -1$. To summarize, we can trust the shape of the AH critical line of $\sigma = +1$ for arbitrary L and that of $\sigma = -1$ for $L \lesssim 0.3$ with the error discussed above.

Figure 19 shows the parameter regions in the (L, j) -plane that allows the AH formation on the new slice in the cases $\sigma = \pm 1$, together with that on the old slice. In both cases, $j_{\text{crit}}^{(\sigma)}(L)$ goes to zero in the limit $L \rightarrow 0$. The

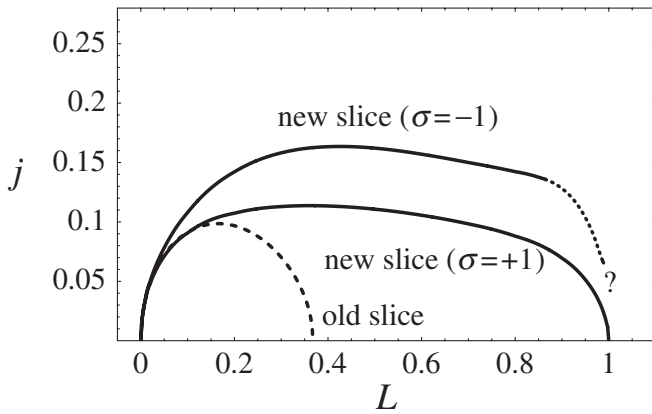


FIG. 19. The critical lines for the AH formation for the new slice for $\sigma = +1$ (lower solid line) and for $\sigma = -1$ (upper solid line). The critical line for the old slice is also shown (dashed line). In both cases $\sigma = \pm 1$, the AH formation is allowed in a larger region on the (L, j) -plane compared to the old slice. The allowed region of $\sigma = -1$ is larger than that of $\sigma = +1$. In the case $\sigma = -1$, the perturbative quantity becomes large at $L \gtrsim 0.9$ and the shape of the critical line cannot be trusted there (dotted line).

critical line of $\sigma = +1$ crosses the L -axis at $L = 1$, which is much larger compared to $L = 1/e$ in the case of the old slice. Although the error in $j_{\text{crit}}^{(-)}(L)$ grows large for $L \gtrsim 0.9$, the critical line of $\sigma = -1$ does not seem to cross the L -axis for $0 \leq L < 1$. Hence, the allowed regions of the new slice is much larger than that of the old slice for both $\sigma = \pm 1$. At the end of the previous section, we stated our expectation that the large difference between the allowed regions of the (2a) and (2b) cases is due to the artificial effect of the slice choice. It is now confirmed, since the allowed region of the (2b) case has become much larger by just changing the slice. Comparing the two cases $\sigma = \pm 1$, $j_{\text{crit}}^{(-)}(L)$ is greater than $j_{\text{crit}}^{(+)}(L)$. Therefore, the AH formation in the case $\sigma = -1$ is allowed in a larger parameter region compared to the case $\sigma = +1$, and the condition of the AH formation depends on the relative helicities of incoming gyratons. To briefly summarize, on the new slice, the condition of the AH formation is roughly expressed as $L \sim 0.5$ and $j \lesssim 0.1$ in the case $\sigma = +1$ and $L \sim 0.5$ and $j \lesssim 0.15$ in the case $\sigma = -1$.

The reason why the allowed region in the case $\sigma = +1$ is limited to $0 \leq L \leq 1$ is understood as follows. In the case $j = 0$, the AH solution is given by

$$\begin{aligned} h^{(1)}(r) = h^{(4)}(r) &= L + 2r^2 \log(r/r_{12}), \\ (r_{12} \leq r &\leq \sqrt{e}r_{12}), \end{aligned} \quad (90)$$

$$h^{(2)}(r) = h^{(3)}(r) = 2 \log(r/r_{12}), \quad (r_{12} \leq r \leq 1), \quad (91)$$

with $r_{12} = 1/\sqrt{L}$. Although the AH is expected to converge to this solution in the limit $j \rightarrow 0$, we should take care of the presence of the singularity $uv = r^2$, where the perturbative quantities diverge. For $L > 1$, the singularity crosses the surface (91), invalidating it to be an AH. Hence $j = 0$ and $j = 0_+$ are different for $L > 1$, and no AH exists for small j . On the other hand, for $0 \leq L \leq 1$, the surface

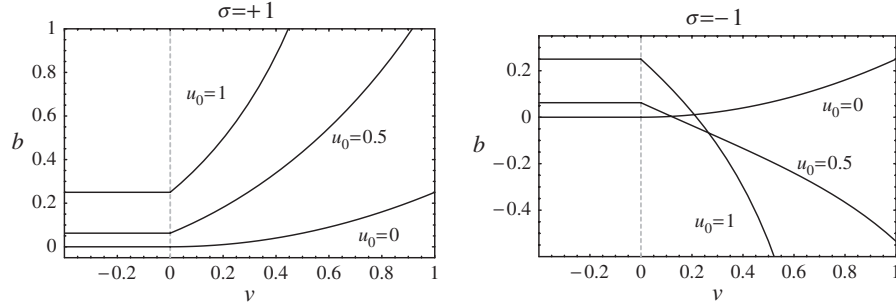


FIG. 20. The behavior of the function $b(u_0, v, r_0)$ in the cases $\sigma = +1$ (left) and $\sigma = -1$ (right) for $r_0 = 1$ and $u_0 = 0, 0.5, 1$. The value of $b(u_0, v, r_0)$ is directly related to the radius $r_{\text{loop}}^{(u_0, r_0)}(v)$ of the light ray congruence $u = u_0, r = r_0, 0 \leq \phi \leq 2\pi$. The light rays quickly bend at $v = 0$ due to the delta functions in Riemann curvature (78) and (79) in both cases but the bending directions are opposite. $b(u_0, v, r_0)$ continues to increase in the case $\sigma = +1$, while its behavior strongly depends on u_0 in the case $\sigma = -1$.

(90) and (91) is the AH in the limit $j \rightarrow 0$, because the singularity does not cross the surface. Hence, it is natural that the region of the AH formation is restricted to $0 \leq L \leq 1$. Although we could not specify the allowed region for $\sigma = -1$ around $L \approx 1$, the above discussion would hold also for this case. Hence, if the exact solution for region IVA is found, the allowed region for $\sigma = -1$ will turn out to be restricted to $0 \leq L \leq 1$.³

D. Gravitational field in the region IVA

We discuss the properties of gravitational field in region IVA in more detail, because it helps us to understand the reason for the different allowed regions in the cases $\sigma = \pm 1$. For this purpose, we study the “gravitational force” acting on the null geodesics $u, r, \phi = \text{const}$ and $v, r, \phi = \text{const}$.

Let us consider a null geodesic congruence $u = u_0, r = r_0, 0 \leq \phi \leq 1$. The section of the congruence and $v = \text{const}$ is a loop and the quantity

$$r_{\text{loop}}^{(u_0, r_0)}(v) = r_0(1 + \epsilon^2 b(u_0, v, r_0)/2) \quad (92)$$

gives a radius of the loop (i.e., the proper circumference divided by 2π). We define the “gravitational force” $F^{(u_0, r_0)}(v)$ toward the symmetry axis by

$$F^{(u_0, r_0)}(v) := \frac{\partial^2 r_{\text{loop}}^{(u_0, r_0)}}{\partial v^2}. \quad (93)$$

The force is attractive if $F^{(u_0, r_0)}(v) < 0$ and repulsive if $F^{(u_0, r_0)}(v) > 0$. Similarly we consider another congruence $v = v_0, r = r_0, 0 \leq \phi \leq 1$ and introduce its loop radius $r_{\text{loop}}^{(v_0, r_0)}(u)$. Then another kind of force is defined by

³This discussion holds only for a collision of gyratons with singular sources, Eqs. (3) and (4). In the collision of realistic beam pulses, the singularity is not produced at $uv = r^2$ and the regions of AH formation might become different from Fig. 19.

$$F^{(v_0, r_0)}(u) := \frac{\partial^2 r_{\text{loop}}^{(v_0, r_0)}}{\partial u^2}. \quad (94)$$

The two forces are calculated as

$$F^{(u, r)}(v) = \frac{\epsilon^2}{4r^3} \left[2\sigma u \delta(v) + 1 + \sigma \frac{u^2(3-x)}{r^2(1-x)^3} \right], \quad (95)$$

$$F^{(v, r)}(u) = \frac{\epsilon^2}{4r^3} \left[2\sigma v \delta(u) + 1 + \sigma \frac{v^2(3-x)}{r^2(1-x)^3} \right]. \quad (96)$$

The delta function of the first term in the square brackets of each formula comes from the new shock field at $u = 0 \leq v \leq L$ and $v = 0 \leq u \leq L$ [see Eqs. (78) and (79)].

In the case $\sigma = +1$, both $F^{(u, r)}(v)$ and $F^{(v, r)}(u)$ are positive outside of the singularity $x = 1$. Hence, the gravitational field is repulsive in the whole region IVA. On the other hand, in the case $\sigma = -1$, the coefficients of the delta functions in Eqs. (95) and (96) are negative, indicating that the new shock fields are attractive. The third term in the square brackets is also negative. If x is close enough to 1, the third term exceeds the second term and the force becomes negative. Hence, around the singularity $x = 1$, there is always the attractive region of the gravitational force. If x is close to 0, the third term is smaller than 1 and the gravitational field is repulsive in such a region. Therefore, both attractive and repulsive regions exist for $\sigma = -1$.

Let us look at the behavior of the loop radius $r_{\text{loop}}^{(u_0, r_0)}(v)$. Ignoring a factor, the change in $r_{\text{loop}}^{(u_0, r_0)}(v)$ is presented by $b(u_0, v, r_0)$. Figure 20 shows the behavior of $b(u_0, v, r_0)$ for $r_0 = 1$ and $u_0 = 0, 0.5, 1$ for the two cases $\sigma = \pm 1$. Because of the delta function in the force (95), $b(u_0, v, r_0)$ is not smooth at $v = 0$ for $u_0 > 0$ in both cases. In the case $\sigma = +1$, $b(u_0, v, r_0)$ suddenly increases at $v = 0$ and blows up, since the force is repulsive everywhere. In the case $\sigma = -1$, $b(u_0, v, r_0)$ suddenly decreases at $v = 0$ due to the attractive force. For $v > 0$, the behavior of $b(u_0, v, r_0)$ strongly depends on the value of u_0 . If u_0 is

large, the light ray feels repulsive force at the beginning but later feels attractive force.

Now we discuss the reason for $j_{\text{crit}}^{(-)}(L) \geq j_{\text{crit}}^{(+)}(L)$, i.e., the difference between the allowed regions for the AH formation of $\sigma = \pm 1$. In the case $\sigma = +1$, the gravitational field in region IVA is repulsive everywhere. If j is increased, the repulsive force exceeds the attractive force generated by the energy, causing the disappearance of the trapped region. On the other hand, in the case $\sigma = -1$ there are both attractive and repulsive regions. Figure 21 shows the sign of two forces $F^{(u,r)}(v)$ and $F^{(v,r)}(u)$ on slice (2), i.e. $0 \leq v \leq L = u$. The slice is divided into three regions: region (--) where $F^{(u,r)}(v) < F^{(v,r)}(u) < 0$, region (-+) where $F^{(u,r)}(v) < 0 < F^{(v,r)}(u)$, and region (++) where $0 < F^{(u,r)}(v) < F^{(v,r)}(u)$. This figure shows that the gravitational force is attractive around the singularity $x = 1$ and repulsive for $r \gg L$. For $L \ll 1$, the attractive region is a tiny portion just around the singularity and the force is repulsive almost everywhere on the surface. The repulsive force becomes dominant as j is increased, resulting in disappearance of the AH. Although the attractive region becomes large for $L \simeq 1$, the attractive force does not help the AH formation effectively since there is the constraint $j_{\text{crit}}^{(-)}(L = 1) = 0$ coming from the size of the singularity $x = 1$ as discussed in the previous subsection. Therefore, also in the case $\sigma = -1$, the spin j makes the AH formation more difficult. However, in the case $\sigma = -1$, the repulsive force is obviously smaller than that of the case $\sigma = +1$ for a fixed j value. Hence, a larger value of j is needed for the disappearance of the AH. This explains our result $j_{\text{crit}}^{(-)}(L) \geq j_{\text{crit}}^{(+)}(L)$.

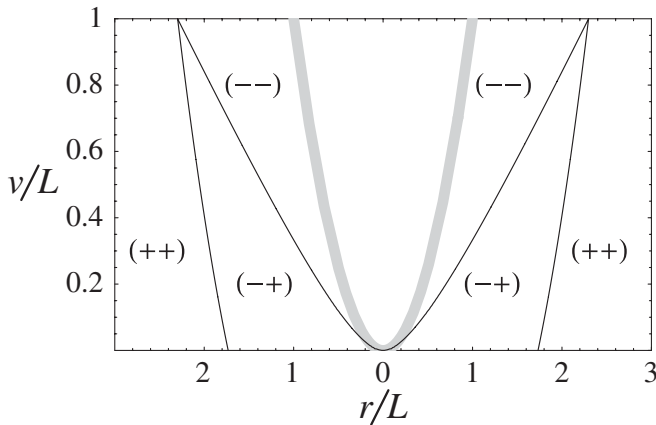


FIG. 21. The sign of two forces $F^{(u,r)}(v)$ and $F^{(v,r)}(u)$ on slice (2), i.e. $0 \leq v \leq L = u$, for $\sigma = -1$. The slice is divided into three regions: region (--) where $F^{(u,r)}(v) < F^{(v,r)}(u) < 0$, region (-+) where $F^{(u,r)}(v) < 0 < F^{(v,r)}(u)$, and region (++) where $0 < F^{(u,r)}(v) < F^{(v,r)}(u)$. The unit of r (horizontal line) and the unit of v (vertical line) is the spin duration L and the gray line indicates the singularity $x = 1$.

VI. SUMMARY AND DISCUSSION

In this paper, we studied the AH formation in the head-on collision of gyratons. We introduced four gyraton models in Sec. II: a spinless p -gyraton, an AS-gyraton, and spinning a - and b -gyratons. The energy and spin profiles of each gyraton are given in Eqs. (7)–(10). For a spinless p -gyraton and an AS-gyraton, the energy profile is a step function with width L and a delta function, respectively. For a - and b -gyratons, the energy profile is a delta function and the spin profile is a step function with width L . The difference between a - and b -gyratons is the relative locations of the energy and spin profiles. We introduced the null geodesic coordinates for each gyraton, and discussed the property of its gravitational field. Especially, a spinning gyraton has a repulsive gravitational field around its center.

Then the problem of the head-on collisions of two gyratons was set up and the AH was studied on the slice $u = 0 \geq v$ and $v = 0 \geq u$ in Secs. II, III, and IV. The studied collision cases and obtained results are summarized in Table I. In all cases two gyratons are assumed to have the same energy. Case (0) is the collision of two identical spinless p -gyratons. In this case the energy duration L should be smaller than some critical value for the AH formation. In cases (1a) and (1b), we studied the collision of spinning a - and b -gyratons with an AS-gyraton, respectively. We obtained the conditions for the AH formation in terms of the spin duration L and the spin j . They are shown in Fig. 10 and roughly summarized as in Table I. (Here $j > 0$ is assumed since the AH formation does not depend on the spin direction.) In both cases, there was a critical value $j_{\text{crit}}(L)$ for the AH formation for a given L . We found no significant difference between the two cases. In cases (2a) and (2b), we studied the collision of two spinning a - and b -gyratons, respectively. Two gyratons were assumed to have the same spin duration L and absolute value of the spin j . We obtained the conditions for AH formation in terms of L and j . They are shown in Fig. 13 and roughly summarized as in Table I. (Here $j > 0$ is assumed and the relative direction of two spins σ is not specified, since the AH formation does not depend on the directions of two spins on the studied slice.) We found that the allowed region on the (L, j) -plane in the (2b) case is much smaller than that in the (2a) case.

In Sec. V, we focused our attention on the gravitational spin-spin interaction after collision in the (2b) case. We solved a part of the future to the slice $u = 0 \leq v$ and $v = 0 \leq u$ (old slice) in the collision of gyratons with spins j and σj ($\sigma = \pm 1$), using a method of perturbation where j is a small expansion parameter. The solved region is the past to the collision of the energy flows, but the two spin flows interact with each other in that region (see Fig. 14 for details). Therefore we could study the spin-spin interaction. Then we again studied the AH formation on the future edge of the solved region (new slice) and compared the obtained results to those of the old slice. It was found that

TABLE I. Summary of the obtained results. For each case, the condition of AH formation was found in terms of L [the energy duration in the (0) case and the spin duration in other cases] and the spin value $j = J/2pr_h(2p)$ (assumed to be positive). The unit of the length is $r_h(2p) = 4Gp$.

Collision type	Slice (σ)	Gyraton 1	Gyraton 2	Condition of AH formation	
(0)	\dots	p	p	$L \lesssim 1.4$	
(1a)	\dots	a	AS	$L \sim 1$	$j \lesssim 0.25$
(1b)	\dots	b	AS	$L \sim 1$	$j \lesssim 0.25$
(2a)	\dots	a	a	$L \sim 1$	$j \lesssim 0.2$
(2b)	Old	b	b	$L \sim 0.15$	$j \lesssim 0.1$
(2b)	New (+1)	b	b	$L \sim 0.5$	$j \lesssim 0.1$
(2b)	New (-1)	b	b	$L \sim 0.5$	$j \lesssim 0.15$

the allowed region becomes larger by just changing the slice (Fig. 19). Hence, the difference between the results of old slice in cases (2a) and (2b) was due to the artificial effect of choosing a slice on which we study the AH.

Furthermore, we found the dependence on the relative helicities of incoming gyratons. In the case $\sigma = +1$ where two spins have the same direction (i.e., helicities have opposite signs), the gravitational field is repulsive everywhere due to the spin-spin interaction. On the other hand, in the case $\sigma = -1$ where two spins have the opposite directions (i.e., helicities have the same sign), the spin-spin interaction decreases the repulsive force and even changes it into the attractive force in a part of the studied region. Correspondingly the allowed region of the AH formation for $\sigma = -1$ is larger than that for $\sigma = +1$ (Fig. 19).

In the light of the above studies, we claim the following. For the AH formation in the head-on collision of gyratons: (i) the energy duration should be smaller than some critical value (close to the system gravitational radius); (ii) the spin duration should be at least of order of the system gravitational radius (it should not be too small or too large); (iii) the spin should be smaller than some critical value that is a function of the spin duration. Further, (iv) the AH formation in the collision of two gyratons with the oppositely directed spins is easier than that with the same direction of spins.

Now we discuss the possible applications of the obtained results for mini-black-hole production at the LHC in the TeV gravity scenarios where $M_p = \text{TeV}$. Let us consider the collision of two spinning particles, and use our result of the (2a) case, i.e. the collision of two identical a -gyratons, for the condition for the black hole formation as an example. Restoring the length unit, it is written as $L \simeq r_h(2p)$ and $J \lesssim 0.4 \times pr_h(2p)$. We use the Lorentz contracted proton size $L \sim 1.5 \times 10^{-4}$ fm for the spin duration and put $J = \hbar/2$ as possible candidates for these values. Substituting $p = (\text{few})M_p$ and $r_h(2p) = (\text{few})\hbar/M_p$, we find $L \sim r_h(2p)$ and

$$0.4 \times pr_h(2p) \sim (\text{few})\hbar \gtrsim \hbar/2 = J. \quad (97)$$

Hence, the above two conditions are satisfied and the black

hole is expected to form in the head-on collision under our assumption. Thus, the effect of spins of incoming particles might not be significant for the black hole production rate. Still, the spin might change the cross section of the black hole production by a factor and studying this effect would be interesting.

We also revisit the study by Giddings and Rychkov [11], because our study is related to the assumption they made. In that paper the collision of quantum wave packets with width L was considered. Their result is that if $\hbar^2/(r_h M_p^2) \ll L \ll r_h$, the higher-curvature correction is small and the predictions by general relativity are reliable. The latter inequality $L \ll r_h$ was imposed by the expectation that the gravitational field of such a wave packet would be sufficiently close to that of the AS particle and thus the AH would form in a collision of such two wave packets. Our result of the (0) case, i.e. the collision of two identical p -gyratons, explicitly demonstrates the accuracy of this expectation. Moreover, because we found the AH also for $L \lesssim 1.4r_h$, the condition can be relaxed to $\hbar^2/(r_h M_p^2) \ll L \lesssim r_h$. Note that this criterion holds also for wave packets of spinning particles, if their energy is sufficiently large, $p \gg M_p$. Our results of the (2a) and (2b) cases, i.e. the collisions of two identical spinning a - and b -gyratons, show that $j^2 \lesssim L$ is necessary for the AH formation for small L . Restoring the length unit and adopting $J = \hbar/2$, it is rewritten as $\hbar^2/(16r_h p^2) \lesssim L$. However, this does not provide a new condition since the original condition $\hbar^2/(r_h M_p^2) \ll L$ implies $\hbar^2/(16r_h p^2) \lesssim L$ for $p \gg M_p$. Therefore, our results do not contradict the claims in [11].

The important remaining problems are as follows. The first one is to explore the case $\sigma = -1$ further. This is because the condition of the black hole formation is expected to be different from that of the AH formation. In the case $\sigma = +1$, however, the critical value of j for the black hole formation will remain finite, because both the gravitational field generated by the spin source and the spin-spin interaction are repulsive. On the other hand, in the case $\sigma = -1$, the repulsive gravitational field of each incoming gyraton is weakened and becomes even attractive in some part of the spacetime by the spin-spin interaction as shown in Sec. IV. Hence, there is the possibility that later the

gravitational field turns to be attractive everywhere and the critical value of j blows up.

The next problem is the collision of gyratons with a nonzero impact parameter. In these grazing collisions, new effects of the spin-orbit interaction will appear. Moreover, the properties of spin-spin interaction might change. Let us recall Eq. (62), the acceleration \vec{a}_{SS} due to the spin-spin interaction between weakly gravitating bodies. In the grazing collisions, the spins are orthogonal to the relative location vector and \vec{a}_{SS} is calculated as $\vec{a}_{SS} = -(3/\mu r^4) \times (\vec{S}_1 \cdot \vec{S}_2)\vec{n}$. Therefore in the aligned (respectively antialigned) case, the spin-spin interaction becomes attractive (respectively repulsive), which is opposite to the head-on collision case. Therefore it is expected that the nonzero impact parameter would make the interactions more complicated but more interesting.

It is also important to simulate the collision of gyratons with realistic sources. In this paper, we assumed that each incoming gyration has a singular source, Eqs. (3) and (4), and studied only the spacetime regime where the matter

interaction is not important (i.e., $uv < r^2$ in Sec. V). In a realistic situation, however, the source of an incoming gyration is a beam pulse with a finite radius \bar{r}_s . Then, the matter interaction determines the spacetime structure within the light cone of the source collision, and the condition for the black hole formation will depend on the properties of matter interaction. In order to study this effect, we should solve the Einstein equations together with the field equations for the sources.

Finally, the generalization for the higher-dimensional case is necessary to obtain the results that can be directly applied for the black hole production at accelerators in the TeV gravity scenarios.

ACKNOWLEDGMENTS

H. Y. thanks Tetsuya Shiromizu for helpful discussions at the early stage of this work. The authors thank the Killam Trust for financial support. One of the authors (V.F.) is grateful to the NSERC for its support.

-
- [1] N. Arkani-Hamed, S. Dimopoulos, and G. R. Dvali, Phys. Lett. B **429**, 263 (1998); I. Antoniadis, N. Arkani-Hamed, S. Dimopoulos, and G. R. Dvali, *ibid.* **436**, 257 (1998).
 - [2] L. Randall and R. Sundrum, Phys. Rev. Lett. **83**, 3370 (1999).
 - [3] L. Randall and R. Sundrum, Phys. Rev. Lett. **83**, 4690 (1999).
 - [4] T. Banks and W. Fischler, arXiv:hep-th/9906038; S. B. Giddings and S. Thomas, Phys. Rev. D **65**, 056010 (2002); S. Dimopoulos and G. Landsberg, Phys. Rev. Lett. **87**, 161602 (2001).
 - [5] D. M. Eardley and S. B. Giddings, Phys. Rev. D **66**, 044011 (2002).
 - [6] P. C. Aichelburg and R. U. Sexl, Gen. Relativ. Gravit. **2**, 303 (1971).
 - [7] H. Yoshino and Y. Nambu, Phys. Rev. D **67**, 024009 (2003).
 - [8] H. Yoshino and V. S. Rychkov, Phys. Rev. D **71**, 104028 (2005).
 - [9] H. Yoshino and R. B. Mann, Phys. Rev. D **74**, 044003 (2006).
 - [10] D. M. Gingrich, J. High Energy Phys. **02** (2007) 098.
 - [11] S. B. Giddings and V. S. Rychkov, Phys. Rev. D **70**, 104026 (2004).
 - [12] V. P. Frolov and D. V. Fursaev, Phys. Rev. D **71**, 104034 (2005).
 - [13] V. P. Frolov, W. Israel, and A. Zelnikov, Phys. Rev. D **72**, 084031 (2005).
 - [14] V. P. Frolov and A. Zelnikov, Classical Quantum Gravity **23**, 2119 (2006).
 - [15] V. P. Frolov and F. L. Lin, Phys. Rev. D **73**, 104028 (2006).
 - [16] V. P. Frolov and A. Zelnikov, Phys. Rev. D **72**, 104005 (2005).
 - [17] M. M. Caldarelli, D. Klemm, and E. Zorzan, Classical Quantum Gravity **24**, 1341 (2007).
 - [18] C. O. Loustó, and N. Sánchez, Nucl. Phys. **B383**, 377 (1992).
 - [19] H. Balasin and H. Nachbagauer, Classical Quantum Gravity **11**, 1453 (1994); **12**, 707 (1995); **13**, 731 (1996).
 - [20] C. Barrabès and P. A. Hogan, Phys. Rev. D **64**, 044022 (2001); **67**, 084028 (2003); **70**, 107502 (2004).
 - [21] H. Yoshino, Phys. Rev. D **71**, 044032 (2005).
 - [22] V. S. Rychkov, Phys. Rev. D **70**, 044003 (2004).
 - [23] R. Wald, Phys. Rev. D **6**, 406 (1972).
 - [24] E. Guadagnini, Phys. Lett. B **548**, 19 (2002).
 - [25] A. Barbieri and E. Guadagnini, Nucl. Phys. **B719**, 53 (2005).
 - [26] B. M. Barker and R. F. O'Connell, Phys. Rev. D **12**, 329 (1975).
 - [27] K. S. Thorne and J. B. Hartle, Phys. Rev. D **31**, 1815 (1985).
 - [28] D. A. Leahy and W. G. Unruh, Phys. Rev. D **19**, 3509 (1979).
 - [29] A. Vilenkin, Phys. Rev. D **20**, 1807 (1979).
 - [30] P. A. Bolashenko and V. P. Frolov, Teor. Mat. Fiz. **78**, 45 (1989) [Theor. Math. Phys. (Engl. Transl.) **78**, 31 (1989)].
 - [31] D. Ida, K. y. Oda, and S. C. Park, Phys. Rev. D **67**, 064025 (2003); **69**, 049901(E) (2004).